Tectonic and climatic control on terrace formation: coupling in situ produced ^{10}Be depth profiles and luminescence approach, Danube River, Hungary, Central Europe

Zsófia Ruszkiczay-Rüdiger[1], Régis Braucher[2], Ágnes Novothny[3], Gábor Csillag[4], László Fodor[5], Gábor Molnár[5], Balázs Madarász[6] & ASTER Team*[2]

[1] *Hungarian Academy of Sciences (MTA); Research Centre for Astronomy and Earth Sciences, Institute for Geological and Geochemical Research, Budaörsi út 45. 1112 Budapest, Hungary, rzsofi@geochem.hu*

[2] *Aix-Marseille University, CEREGE, CNRS-IRD UM34, BP 80, 13545 Aix-en-Provence Cedex 4, France. braucher@cerege.fr*

[3] *Department of Physical Geography, Eötvös University, Pázmány P. sétány 1/C, 1117, Budapest, Hungary, agnes.novothny@gmail.com*

[4] *Geological and Geophysical Institute of Hungary, Stefánia út 14, 1143, Budapest, Hungary, csillag.gabor@mfgi.hu*

[5] *MTA-ELTE Geological, Geophysical and Space Research Group of the Hungarian Academy of Sciences at Eötvös University, Pázmány P. sétány 1/C, 1117, Budapest, Hungary, lasz.fodor@yahoo.com, molnar@sas.elte.hu*

[6] *Hungarian Academy of Sciences (MTA); Research Centre for Astronomy and Earth Sciences, Geographical Institute, Budaörsi út 45. 1112 Budapest, Hungary,* madaraszb@sparc.core.hu

* *Maurice Arnold (arnold@cerege.fr), Georges Aumaître (aumaitre@cerege.fr), Didier Bourlès (bourles@cerege.fr), Karim Keddadouche (keddadouche@cerege.fr)*

Abstract

The terrace sequence of the Hungarian part of the Danube valley preserves a record of varying tectonic uplift rates along the river course and throughout several climate stages. To establish the chronology of formation of these terraces, two different dating methods were used on alluvial terraces: exposure age dating using in situ produced cosmogenic ^{10}Be and luminescence dating. Using Monte Carlo approach to model the denudation rate-corrected exposure ages, in situ produced cosmogenic ^{10}Be samples originated from vertical depth profiles enabled the determination of both the exposure time and the denudation rate. Post-IR

IRSL measurements were carried out on K-feldspar samples to obtain the ages of sedimentation.

The highest terrace horizon remnants of the study area provided a best estimate erosion-corrected minimum ^{10}Be exposure age of >700 ka. We propose that the abandonment of the highest terrace of the Hungarian Danube valley was triggered by the combined effect of the beginning tectonic uplift and the onset of major continental glaciations of Quaternary age (around MIS 22). For the lower terraces it was possible to reveal close correlation with MIS stages using IRSL ages. The new chronology enabled the distinction of tIIb (~90 ka; MIS 5b-c) and tIIIa (~140 ka; MIS 6) in the study area. Surface denudation rates were well constrained by the cosmogenic ^{10}Be depth profiles between 5.8 m/Ma and 10.0 m/Ma for all terraces. The calculated maximum incision rates of the Danube relevant for the above determined >700 ka time span were increasing from west (<0.06 mm/a) to east (<0.13 mm/a), toward the more elevated Transdanubian Range. Late Pleistocene incision rates derived from the age of the low terraces (~0.13-0.15 mm/a) may suggest a slight acceleration of uplift towards present.

Keywords: cosmogenic ^{10}Be exposure age, depth profiles, denudation rate, post-IR IRSL, river terrace, incision rate, uplift rate, Quaternary

1. Introduction

The age and position of a fluvial terrace with respect to a reference level provides a good approximation of the river incision rate. In certain occasions this is a valid time-averaged proxy for the surface uplift rate. On the other hand, climatically induced changes in river style can also lead to terrace formation (Bridgland, 2000; Peters and Van Balen, 2007; Bridgland and Westaway, 2008; Gibbard and Lewin, 2002, 2009; Warner, 2012). Incision/uplift rates calculated on the basis of age determination of river terraces in Europe mostly suggest values up to ~1 mm/a for middle and late Pleistocene times (Brocard et al., 2003; Peters and van Balen, 2007; Viveen et al., 2012; Necea et al., 2013; Rixhon et al, 2011, 2014) and exceptionally, in tectonically active regions, like the SE Carpathians (Necea et al., 2013) or for shorter periods (Antón et al., 2012) present higher rates. Burial age determination of cave sediments using cosmogenic ^{10}Be and ^{26}Al in Schwitzerland suggested an incision rate of 0.12 mm/a for the early Pleistocene, and a tenfold increase was suggested for middle to late Pleistocene times Häuselmann et al. (2007a). Applying the same method Wagner et al. (2010)

calculated rather low average bedrock incision rates of 0.1 mm/a for the last 4 Ma with a decreasing trend towards present (Table 1). However, the decrease towards younger times was attributed to the rise of the base level due to sediment aggradation within the valley.

The uplift rate of 1.75 mm/a provided by geodetic measurements in the western and northern Alpine foreland (Ziegler and Dézes, 2007) represents the higher end of the uplift rates based on geochronological and geomorphological constraints (Table 1)

The combined application of cosmogenic ^{10}Be exposure dating and luminescence dating allows a more robust age determination than using either method separately, as it was demonstrated by some previous studies (Anders et al, 2005; Delong and Arnold, 2007; Guralnik, 2011; Viveen et al., 2012). Main objective of the present study is to provide age constraints to fluvial terraces of the Danube River in order to determine its incision rate. New constraints on vertical neotectonic deformation of the western Pannonian Basin and on the role of climate change in terrace evolution are presented. Denudation rates provided by ^{10}Be depth profiles will contribute to a better understanding of the pace of surface processes in the region.

2. Geological and geomorphological setting

2.1. Quaternary tectonics and drainage pattern evolution

The Pannonian Basin (Fig. 1) represents a back-arc basin formed by Miocene crustal thinning and subsequent "post-rift" thermal subsidence (Horváth and Royden, 1981, Horváth et al. 2015), which led to the formation of the several 100 m deep Lake Pannon. This lake was filled up during the late Miocene due to large sediment input (Magyar et al., 2007, 2013). The Western Pannonian Basin was subsequently occupied by a fluvio-lacustrine system, established in the latest Miocene (Uhrin et al., 2011), with paleo-rivers drained towards the south (Szádeczky-Kardoss 1938, 1941; Pécsi, 1959; Gábris and Nádor, 2007). Neotectonic shortening and related uplift progressively shifted from SW (Slovenia) toward NE (Tari, 1994; Fodor et al. 2005). The deflection of the Alpine and Carpathian rivers (including the paleo-Danube) from their southerly flow towards the east, their current runoff direction, followed the propagation of the neotectonic deformation. As a result, the formation of a large alluvial fan in the Danube Basin was proposed during the early Pleistocene (Szádeczky-Kardoss, 1938, 1941) (Fig. 2), and the Danube was forced to find its way towards the east

across the TR. The age of abandonment of the highest terrace of the Danube provides a good approximation of the age of the onset of fold-related uplift in the northeast part of the TR.

Neotectonic structures developed due to changing boundary conditions of the deformation: one of the major driving forces, the eastward pull (subduction rollback) beneath the Eastern Carpathians largely decreased while northward push of the Adriatic plate continued (Horváth, 1995, Bada et al., 2006). In the new neotectonic regime transpression resulted in the reactivation of strike slip faults and large-scale folding of the Pannonian lithosphere manifested by the coexistence of several uplifting regions and areas of subsidence (Horváth and Cloetingh 1996, Bada et al., 2006, Ruszkiczay-Rüdiger et al., 2007; Dombrádi et al., 2010). One of these uplifting areas is the SW-NE trending, 300-700 m above sea level (asl) high Transdanubian Range (TR) emerging between the Danube Basin and the Great Hungarian Plain, two lowlands of continuous sediment accumulation since middle Miocene times (Fig.1).

The Danube River is the only one cutting through the uplifting basement unit of the TR (Fig. 1). The differential uplift across the TR, i.e. gradually decreasing uplift rates from its axis towards the neighbouring lowlands, led terrace remnants in the Danube valley to perform an upwarped pattern relative to the modern river profile (Fig. 2; Pécsi, 1959; Gábris, 1994; Ruszkiczay-Rüdiger et al., 2005a; Gábris and Nádor, 2007; Gábris et al. 2012 and references therein). As a consequence, number and position of terraces alter along the Danube and geomorphic horizons of the same age may occur at different elevations across the uplifting range. Moreover, this setting enabled the simultaneous development of fill terraces in the margins, and of strath terraces in the central part of the TR; rising additional difficulty in correlating terrace horizons along the river.

The uplift rates inferred from the published terrace chronological data (Ruszkiczay-Rüdiger et al., 2005a) along the Hungarian segment of the Danube valley varied between 0.05 and 0.36 mm/a at the margins and at the axis of the TR, respectively. ^{3}He surface exposure dating of strath terraces at the Danube Bend (Fig. 1) suggested a maximum incision rate of 1.6 mm/a at the valley section of most intensive uplift, at the NE-SW trending axis of the Transdanubian Range (TR) (Ruszkiczay-Rüdiger et al., 2005b). However, according to GPS velocity measurements the maximum uplift rate in the TR does not exceed 0.5 mm/a (Grenerczy et al., 2005 and pers. comm. 2014).

Our study area, the Győr-Tata terrace region (GTT) is located in the south-eastern margin of the Danube Basin, in the transitional zone of the subsiding area towards the uplifting TR (Figs 1, 2A, 3). Although the regional structural and geomorphological context of the

transitional zone between the Danube Basin and the TR is relatively clear, the local structural setting of the GTT has not been clearly documented. The axis of uplift of the TR is NE-SW (Fig. 1) which is oblique to the present (and postulated Quaternary) direction of compression derived from stress data (Horváth and Cloetingh, 1996; Bada et al. 2006). This gentle folding would lead to westward tilt of the western TR foothills, including the study area. A pronounced Late Miocene fault is present at the western margin of the TR (Fodor et al., 2005; Bada et al., 2007; Dombrádi et al., 2010 Figs. 1, 2A), which could be reactivated in the Quaternary. The abundant travertine occurrences (Pécsi, 1959, Ruszkiczay-Rüdiger et al., 2005a; Kele, 2009; Sierralta et al., 2009) along proposed fault may be connected to this reactivation. Our study area, the GTT is situated to the west from this possible Quaternary fault (Figs. 1, 2A).

In the south-western part of the TR ^{10}Be exposure age of wind-eroded landforms was determined up to 1.56±0.09 Ma (Ruszkiczay-Rüdiger et al., 2011) (Fig.1). This age provides a minimum time constraint on the onset of the inversion-related uplift in the southwest part of the TR.

At the same time, during the early Pleistocene, the Danube was already deflected from its southerly flow and formed a large alluvial fan in the subsiding Danube Basin (Fig. 2A; Szádeczky-Kardoss, 1938, 1941). According to Pécsi (1959), in the slightly uplifted TR at least 3 terraces (tVI–tIV) were formed during this period of time (Fig. 3). In the traditional terrace chronology, the tVI horizon is considered to be the first terrace of Danubian origin in the central TR. Recently, the origin of the horizons above tV has been questioned: they might be remnants of surfaces pre-dating the appearance of the Danube River in the area (Szeberényi, 2014). We suggest that the number and age of the terraces might be different along the Danube valley because of the possibility of non-developed and/or completely eroded terrace remnants at diverse valley sections.

When the inversion-related vertical movements propagated towards the north and northeast, the Danube incised into the marginal areas of its alluvial fan and into the underlying late Miocene fluvial and lacustrine sediments, formation of a terrace staircase started at the western and eastern side of the Danube Basin (Figs. 1, 2A,B), while continuous aggradation occurred in the basin interior of ongoing subsidence (Fig. 3). The highest terraces at the western (Parndorf plateau) and eastern sides (GTT) of the Danube Basin (tIV; Figs. 2A. and 3) are supposed to be remnants of this ancient alluvial fan (Szádeczky-Kardoss, 1938, 1941; Pécsi 1959).

Age determination of the Danube terraces at the south-eastern margin of the Danube Basin, the GTT will provide time constraints on the propagation of fold-related uplift of the TR from southwest towards the northeast

2.2. Position and age of the terraces in the Győr-Tata terrace region (GTT)

The ages of Hungarian river terraces have traditionally been correlated to different Alpine glacial stages (Günz, Mindel, Riss Würm; Penck and Brückner, 1909) and are numbered from the youngest/lowest horizon (tI, high floodplain) to the higher/older levels (Pécsi, 1959; Kretzoi and Pécsi, 1982). These ages were based mostly on geomorphological and sedimentological correlations of terraces combined by scattered large mammal findings and rare numerical ages. These "traditional" terrace ages were quantified by Ruszkiczay-Rüdiger et al. (2005a), and ages have been further refined by this study considering the studies of (Lisiecki and Raymo, 2005; Gibbard and Van Kolfschoten, 2005; Nitychoruk et al., 2006; Ehlers and Gibbard, 2007) providing new age constraints on the MIS stages of the Alpine glacial terminology (Fig. 4).

Mean level of the Danube in the GTT is at 109-107 m asl, from west to east; based on EOV (Uniform National Projection of Hungary) 1:10 000 topographic maps. Relative terrace heights (current elevation of the surface of the fluvial material) were calculated respectively (Table 2).

Terraces in the GTT occur only on the southern side of the river. To the north, the river is escorted by a wide alluvial plain extending to the southern flanks of the Carpathians (Figs.1, 2A). The floodplain on the Southern riverside is narrow, flood-free terraces are close to the current river. According to the traditional terrace system of the Danube in Hungary (Pécsi, 1959; Kretzoi and Pécsi, 1982; Gábris, 1994; Ruszkiczay-Rüdiger et al., 2005a, Gábris and Nádor, 2007) five terraces occur in the GTT.

The lowest terrace above the floodplain is tIIa is ~9 m above mean river level (amrl). In the neighbouring Gerecse Hills U/Th dated travertines provided an age of 10-40 ka (Kele, 2009) for this terrace, which is the most continuous horizon along the Danube. There are some Th/U age data available on tIIb (increasing height from 12 m to 22 m amrl. from west to east), clustering around 100-130 ka (summary in Ruszkiczay-Rüdiger et al 2005b, and Kele 2009; Table 1A), however it is still not clear whether this horizon has been deposited by the end of the penultimate glacial or at the beginning of the last glacial phase. Above this level terrace

chronology is even more uncertain. The tIII horizon is apparently missing in the study area, its existence in this valley section has not been verified yet (Figs. 2A, B, 3, 4).

In the western part of the GTT elevation of the tIV horizon is at 35-40 m amrl, and it is an extended flat surface covered by 8-10 m thick gravel. At the easternmost part of the region only small remnants of this terrace horizon, covered by thinned terrace material (0-3m), have remained at an elevation of 80-87 m amrl. According to the traditional terrace chronology (Pécsi, 1959) the terrace level was formed during the Mindel glaciation, which ended after MIS 12 (Gibbard and Kolfschoten, 2005; Lisiecki and Raymo, 2005), providing a minimum terrace age of 420 ka.

Krolopp (1995) described an early to middle Pleistocene malacofauna from the eastern and from the western parts of the tIV (Győr and Grébics, respectively; Fig.2A). The described fauna belongs to the *Viviparus boeckhi biozone* and is indicative of fluvial environment under mild, even warm climate. According to Krolopp (1995) this biozone started around the beginning of the Quaternary (ca. 2.6 Ma) and ended with the Günz/Mindel interglacial, which suggests a minimum age of 540 ka for this terrace (Fig. 4).

Gábris (2008) and Gábris et al. (2012) made an attempt to find a direct link between terrace formation and global climate change and made a compilation of terrace incision and marine oxygen isotope data (MIS), assuming that each incision event could be linked to a MIS Termination. On this basis Gábris (2008) suggested younger ages to each terrace than it has been inferred from the revision of the a traditional terrace chronology based on the Alpine glaciations, and divided the tIII terrace into tIIIa and tIIIb horizons (Fig.4).

The malacofauna of similar age (Krolopp 1995) and sedimentological investigations (heavy mineral composition, pebble lithologies and roundedness Pécsi, 1959) proposed that the different segments of the tIV terrace of gradually increasing elevation belong to a single terrace level and thus they share the same age (Fig. 2A, 3). This is supported also by the DEM derived gentle slope of this horizon (<0.1°) between Győr and Grébics, and is in agreement with the tectonic setting of the GTT between the uplifting TR and the subsiding Danube Basin (Figs. 1, 2A, 3).

Another interesting feature of the highest terrace of the GTT (tIV) is its appearance as isolated terrace remnants bordered by steep slopes on both sides (Fig. 1, 2A,B). Towards the Danube, the terrace riser is facing a lower (tIIb) terrace horizon. However, to the south, similarly steep slope leads into a topographic depression with an elevation of 120-130 m carved into the late-Miocene fluvial-lacustrine sedimentary sequence. We suggest that the coarse alluvial sediments of the Danube have protected the surface of the tIV terrace from

denudation, while to the south of the former alluvial fan of the Danube the loose late Miocene sediments were exposed. After the lowering of the erosion base by the incision of the Danube these uncovered areas were object of faster denudation, and thus the terrace remnants became topographically isolated.

Most important consequence of this topography for surface exposure dating is that the tIV level has been disconnected from potential sediment sources, hence post abandonment sediment accumulation could be disclosed. On the other hand, considerable amount of denudation must have occurred, evidenced by the fact that the fine overbank deposits have been stripped from above the coarse channel or point-bar facies (gravelly sand, sandy gravel) exposed on the present terrace surface.

3. Material and methods

3.1. Sampling strategy

Terrace deposits of the study area consist of cross bedded sandy gravels, gravelly sands. No silt or clay lenses were observed. Low terraces (tIIa and tIIb) were frequently covered by 1-1.5 m thick fine grained alluvial cover, aeolian sand or loess. The most frequent gravel material was quartzite, which was the main target for the sampling in gravel layers. In most cases, imbrication of the pebbles and bedding of the sand indicated original position of the sediment. Obscure bedding or evidences of sediment mixing are detailed in the site descriptions. Large cobbles and boulders were missing from all terraces and terrace material was loose, not cemented.

The accumulation history the radioactive cosmogenic ^{10}Be in terrace sediments may be highly complex. Its accumulation prior to deposition (inheritance), surface denudation, post-depositional sediment mixing and aeolian sediment cover are processes that have to be considered (Brocard et al., 2003; Braucher et al., 2009; Antón et al., 2012; Rixhon et al., 2011).

Because of the high probability of surface denudation since terrace formation and unknown amount of inherited cosmogenic nuclides, we use the cosmogenic ^{10}Be depth profile-approach coupled with luminescence dating. The ^{10}Be depth profiles enable the determination of both denudation rate and exposure age of the terraces by considering all particles, neutrons and muons, involved in the production of ^{10}Be (Siame et al., 2004). In addition, the amount of

inherited ^{10}Be and the bulk density can also be estimated (Anderson et al., 1996; Brocard et al., 2003; Siame et al., 2004; Braucher et al., 2003, 2009). An accurate age determination of depositional surfaces can be achieved (Hedrick et al., 2013; Stange et al. 2013; 2014) as long as ^{10}Be concentrations have not yet reached the steady state, with nuclide production and loss (decay + denudation) in equilibrium. If the profile has reached secular equilibrium, long-term denudation rate and minimum exposure age (integration time) of the profile can be constrained (Lal, 1991; Matsushi et al., 2006). In case of post-depositional sediment mixing no exponential decrease of ^{10}Be concentrations is observed with depth (Ward et al., 2005); in that case, it is problematic to determine a terrace abandonment age using cosmogenic ^{10}Be.

Post IR-IRSL dating is suitable to date the time of sediment burial and provides independent age control on the accumulation of terrace material. It is less sensitive of surface processes than exposure age determination, but the useful time range is shorter and is not applicable on gravels. Accordingly, the combined methodology is suitable for providing robust time constraints on terrace formation.

Elevations and positions of the samples were recorded on the field using hand-held GPS (WGS 84 reference datum) and cross referenced with 1:10 000 topographic maps (Table 2). For sampling along depth profiles active or abandoned gravel pits with terrace material exposed in at least 2 m depth in original position are suitable, which prerequisites were fulfilled by only a limited number of locations. These were taken as sample locations of this study (Fig.5).

The highest, tIV terrace horizon was sampled at three locations at increasing altitudes from west to east (147m Győr; 153m Bana; 194m Grébics; Fig. 2A, 5, Table 2). The tIIb level was sampled at two locations, with somewhat different altitudes (121 m – Ács and 127 m – Mocsa). 20-40 pebbles of 1-5 cm size were collected from each sampled depth. From sand layers whole sand samples were collected (Figs. 5, 6). For site descriptions refer to Supplementary Section 3.1.

One sample was collected from the recent gravel of the Danube at Ács (Dan08-27). This sample consisted of quartzite pebbles, which were processed to measure ^{10}Be concentration of the current load of the river. At this location the terrace IIb lies next to the actual riverbed (Fig. 2A,B).

3.2. Cosmogenic ^{10}Be exposure age dating: theory and laboratory analyses

303 3.2.1. Theoretical considerations

304

305 During the last decade Terrestrial in situ produced Cosmogenic Nuclides (TCN) became a
306 widely used technique for dating geomorphic surfaces and determining denudation rates
307 (Bierman; 1994; Cerling and Craig, 1994; Rixhon et al, 2011; Portenga and Bierman, 2011).
308 Terrestrial in situ produced cosmogenic ^{10}Be is produced within quartz mineral lattice near the
309 Earth's surface (Lal, 1991). Quartz is a mineral abundant in most terraces and datable time
310 span using in situ cosmogenic ^{10}Be covers the entire Quaternary (Lal, 1991; Gosse and Philips
311 2001, Dunai, 2010; Hancock et al., 1999.; Brocard et al., 2003; Wolkowinsky and Granger,
312 2004; Häuselmann et al. 2007b).

313 Three main types of secondary particles are involved in the in situ production of
314 cosmogenic nuclides: fast neutrons (L_n), stopping muons (slow or negative; $L_{\mu slow}$) and fast
315 muons ($L_{\mu fast}$). Assuming that the production and erosion rates remained constant through
316 time, the in situ-production of ^{10}Be is given by the following equation:
317 eq(1):

$$N_{(x,\varepsilon,t)} = \frac{P_{sp}.\exp\left(-\frac{x}{L_n}\right)\left(1-\exp\left(-t\left(\frac{\varepsilon}{L_n}+\lambda\right)\right)\right.}{\frac{\varepsilon}{L_n}+\lambda} + \frac{P_{\mu slow}.\exp\left(-\frac{x}{L_{\mu slow}}\right)\left(1-\exp\left(-t\left(\frac{\varepsilon}{L_{\mu slow}}+\lambda\right)\right)\right.}{\frac{\varepsilon}{L_{\mu slow}}+\lambda}$$

$$+\frac{P_{\mu fast}.\exp\left(-\frac{x}{L_{\mu fast}}\right)\left(1-\exp\left(-t\left(\frac{\varepsilon}{L_{\mu fast}}+\lambda\right)\right)\right.}{\frac{\varepsilon}{L_{\mu fast}}+\lambda} + N_0.\exp\left(-\lambda.t\right)$$

318

319 where N(x,ε,t) is the nuclide concentration function of depth x (g/cm^2), denudation rate ε
320 (g/cm^2/y) and exposure time t (y). Depths were defined at the centre of the sample. P_{sp}, $P_{\mu slow}$,
321 $P_{\mu fast}$ and L_n, $L_{\mu slow}$, $L_{\mu fast}$ are the production rates and attenuation lengths of neutrons, slow
322 muons and fast muons, respectively. L_n, $L_{\mu slow}$, $L_{\mu fast}$ values used in this paper are 160, 1500
323 and 4320 g/cm^2, respectively (Braucher et al., 2003). λ is the radioactive decay constant and
324 N_0 is the inherited nuclide concentration. $P_{\mu slow}$, $P_{\mu fast}$ are based on Braucher et al. (2011).
325 Being aware of the importance of material density on the depth profile modelling results
326 (Braucher et al, 2009, Rodés et al., 2011), bulk densities were determined in the laboratory by
327 weighing mass of 100 cm^3 terrace material in wet and dry state. Resulting values for sand,
328 gravelly-sand and sandy-gravel varied between 1.7 and 2.1 g/cm^3. Measured density of the
329 fine aeolian cover (Ács) was 1.6 g/cm^3. Evidently, it was not possible to fit gravelly material
330 in the 100 cm^3 cylinder perfectly and cobbles could not be represented. Hence, density was set

at slightly higher values as a free parameter, between 1.8 and 2.2 g/cm^3, and considered as constant over depth (Guralnik et al., 2011; Rixhon et al, 2011; Stange et al., 2013).

CosmoCalc add-in for Excel (Vermeesch, 2007) has been used to calculate sample thickness scaling (with an attenuation coefficient of 160 g/cm^2) and atmospheric pressures. Production rates were scaled following Stone (2000) with a sea level high latitude production rate of 4.02±0.36 atoms/g SiO_2/yr. This production rate is the weighted mean of recently calibrated production rates in the Northern Hemisphere (Balco et al., 2009; Fenton et al., 2011; Goehring et al., 2012; Briner et al., 2012).

For all samples the topographic shielding was negligible and therefore not corrected for. Based on Dunai (2001), corrections for geomagnetic variations accounted for less than 5% for the considered time span. Ages and denudation were not corrected for this variation.

During glacials, periglacial semi-arid loess steppe climate prevailed in the study area (Van Vliet-Lanoë et al., 2004; Ruszkiczay-Rüdiger et al., 2015), with significant wind erosion (Sebe et al., 2011), thus no correction of production rates for snow cover was necessary.

According to Cerling and Craig (1994) the effect of an old-growth fir forest on the production rate of cosmogenic ^{3}He is less than 4%. Plug et al. (2007) also concluded that the shielding effect on cosmic irradiation of an old-growth boreal forest is less than 3%. Differences in tree species and moisture content, and the lack of forest vegetation may result in an even smaller correction of the site specific production rate, therefore ^{10}Be production rates were not corrected for the vegetation cover effect.

Concentrations of ^{10}Be can be interpreted either as minimum exposure ages assuming negligible denudation, or as maximum denudation rates. In these simplistic assumptions, inherited TCN concentrations from pre-depositional exposure are neglected. When using depth profiles denudation rate, exposure time and inheritance can be quantified if the TCN concentration decreased exponentially with depth (Siame et al., 2004; Braucher et al., 2009)

3.2.2. Laboratory analysis

Chemical treatments of most samples were carried out at the CEREGE laboratory in Aix en Provence (France) except for the alluvial samples from Ács (Dan13-11 to -18). For these samples crushing and quartz purification were performed in the new TCN Sample Preparation Laboratory of the Institute for Geological and Geochemical Research of the Hungarian Academy of Sciences at Budapest.

Amalgamated pebble samples were crushed and sieved. 90-120 g of the 0.25-1 mm grain size fraction was chemically etched. Sand samples were only sieved (0.25-1 mm) and for fine sand samples (Dan 13-07 to-10) the 125-250 μm fraction was used. ~40 g pure quartz was dissolved in HF in the presence of ^{9}Be carrier (100 μg of 3.025 x 10^{-3} g/g ^{9}Be in-house solution). After substitution of HF by nitric- then hydrochloric acids, ion exchange columns (Dowex 1x8 and 50Wx8) were used to extract ^{10}Be (Merchel and Herpers, 1999). Targets of purified BeO were prepared for AMS (Accelerator Mass Spectrometry) measurement of the ^{10}Be/^{9}Be ratios on ASTER, the French national facility, CEREGE, Aix en Provence (Arnold et al., 2010). These measurements were calibrated against the NIST SRM4325 standard, using an assigned value of $(2.79\pm0.3)\times10^{-11}$ for the ^{10}Be/^{9}Be ratio. Analytical uncertainties (reported as 1σ) include uncertainties on AMS counting statistics, uncertainty on the NIST standard ^{10}Be/^{9}Be ratio, an external AMS error of 0.5% (Arnold et al., 2010) and chemical blank measurement. A ^{10}Be half-life of $(1.387\pm0.01)\times10^{6}$ years (Korschinek et al., 2010; Chmeleff et al., 2010) was used.

3.3. Luminescence dating

3.3.1. Theoretical considerations

Luminescence is a radiometric dating method which provides the burial time of the sediment as its most frequent components – quartz and feldspars – are acting as natural radiation dosimeters (Lian and Roberts, 2006; Wintle, 2008). The previous luminescence signal of the minerals can be completely or partially bleached by sunlight during transportation. The rate of bleaching depends on the type of transportation and transport distance. During aeolian transportation it is very likely that the minerals are completely bleached by sunlight, however fluvial, glacial and marine transport may result in partial bleaching.

The luminescence age of the sample is calculated from the equivalent dose (D_e: the natural absorbed radiation dose [Gy] of the sample) divided by the annual natural ionising radiation dose (dose rate [Gy/ka]) of the sample. Quartz is stimulated by blue light during the measurements and generally known as Optically Stimulated Luminescence (OSL). Feldspars are usually stimulated by infrared radiation, which is termed Infrared Stimulated Luminescence (IRSL) to measure the equivalent dose of the samples (Lian and Roberts 2006; Wintle 2008).

398

399 3.3.2. Experimental setup

400

401 The OSL of quartz has a lower dating limit, therefore it can be applied only on younger
402 samples (< 60-100 ka in Hungary). Therefore, in this study post-Infrared Infrared Stimulated
403 Luminescence (post-IR IRSL) measurements were carried out on K-feldspar samples,
404 comparing the post-IR IRSL 290 and post-IR IRSL 225 signals on the samples. The post-IR
405 IRSL signal of feldspar (Thomsen et al., 2008, Buylaert et al., 2009, 2012, Thiel et al., 2011)
406 usually has a dating limit up to 300 ka (Murray et al., 2014) and it shows negligible fading.
407 The IRSL signal of feldspars suffers from anomalous fading – an unwanted, athermal loss of
408 signal, resulting in age underestimation (Wintle, 1973). However, the post-IR IRSL signals
409 are less affected by fading (Thomsen et al., 2008; Buylaert et al., 2009; Thiel et al., 2011),
410 especially the post-IR IRSL-290 signal (Thiel et al., 2011), which does not need fading
411 correction, although a small fading rate (<1-1.5 %/decade) has been measured (Thiel et al.,
412 2011, 2014; Buylaert et al., 2012; Schatz et al., 2012). The applied post-IR IRSL-290 and -
413 225 (pIRIR-290, pIRIR-225) measurement protocols (Table S1) are described in Thiel et al.
414 (2011) and in Buylaert et al. (2009), respectively.
415 Luminescence samples were taken by pushing metal tubes into the previously cleaned
416 wall. The preparation of luminescence samples was conducted under subdued red light. The
417 coarse-grained fraction of 100-150 μm, or 150-200 μm, or 200-250 μm, or 250-300 μm was
418 extracted from the samples. All samples were treated using 0.1 N hydrochloric acid, 0.01 N
419 sodium-oxalate and 30 % hydrogen peroxide to remove carbonate, clay coatings and organic
420 matter from the samples, respectively. Feldspar and quartz grains were extracted by heavy
421 liquid separation using sodium polytungstate.
422 Luminescence measurements were performed using an automated Risø TL/OSL-DA-20
423 reader at the Department of Physical Geography in the Eötvös Loránd University, Institute of
424 Geography and Geology. The reader is equipped with a bialkali EMI 9235QB photomultiplier
425 tube, IR diodes (λ=875 nm) and a 90Sr/90Y β-source. Schott BG-39 and BG-3 filters were
426 placed in front of the photomultiplier, transmitting wavelengths between 350 and 420 nm.
427 Dose rates were obtained from the potassium, uranium and thorium content (Table S2), as
428 measured by gamma spectrometry fitted with a HPGe (High-Purity Germanium) N-type
429 coaxial detector in the laboratory at the Leibniz Institute for Applied Geophysics, in
430 Hannover. Polypropylene Marinelli beakers were filled with 700 g of the sediment and stored
431 for a minimum period of 4 weeks to allow the 226Rn–222Ra equilibrium to be re-established.

A potassium content of 12.5±1% (Huntley and Baril, 1997) was applied to the K-rich feldspar fraction to account for the internal dose rate. An average a-value of 0.08±0.02 (Rees-Jones, 1995) was used for the feldspar IRSL age calculation. The cosmic radiation was corrected for altitude and sediment thickness (Prescott and Hutton, 1994), assuming a water content of 10±5% for all samples. Dose rate conversion is based upon the factors of Adamiec and Aitken (1998).

3.4. Multielectrode resistivity profiles

Ten 2D multielectrode resistivity profiles (MUEL) were measured on the tIV terrace surface aiming at an insight on the thickness of coarse-grained alluvial material deposited by the paleo-Danube (Geomega, 2004). MUEL profiles enable the distinction among the sediments of different textures down to depths of 40-60 m. The profiles were inverted using RES2DINV software. Topographical data were incorporated to the measured data before inversion and elevation changes were accounted for during the inversion process. The inverted profiles were plotted using a horizontal scale of 1:2000, and vertical scale of 1:1000, thus a vertical exaggeration of 2 was applied. The colour scale has been specifically chosen to help discriminating the coarse grained terrace sediments and the underlying finer grained late Miocene strata. Red and purple colours (ie. resistivities above 160 Ohmm) indicate coarse grain sediments. When these sediments are located near the surface of the tIV terrace, they most probably correspond to the deposits of the ancient Danube.

4. Results

4.1. The cosmogenic ^{10}Be depth profile approach

The time needed to reach the steady state concentration considering muon particles at depth is much longer than at surface, where neutrons are the predominant particles in the total production of cosmogenic nuclides (Braucher et al, 2003). Thus, as a first step, to determine whether a depth profile has reached the secular equilibrium or not, one may assume an infinite exposure age for all samples along the depth profile, then calculate the correlated maximum denudation rates using eq(1) (Table 2). If the denudation rates are increasing from the top to the bottom, then the steady state has not been reached, and an exposure age can be

466 determined. If the denudation rates remain constant implies that steady state has been reached,
467 which allows the determination of a minimum age of terrace abandonment only. When
468 denudation rates are constant until a certain depth and increase below that depth, then the
469 upper part of the profile will fix the denudation rate and the exposure time can be assessed
470 using the bottom part of the profile.
471 Constant or slightly decreasing maximum denudation rates for the Danube profiles at the
472 upper 1.5-2 m (save the Ács profile) suggest steady state conditions at the top (Table 2). The
473 ^{10}Be concentrations, however, become lower for the deepest samples, which may indicate a
474 difference of inherited ^{10}Be inventories. However, this shift of the ^{10}Be concentrations is not
475 reflected by a visible change of the sedimentary succession, as it could be expected in case of
476 a major change in source area, or at a larger time gap within the terrace deposit. At Grébics,
477 maximum denudation rates are constant with depth within uncertainties suggesting steady
478 state for all samples of the profile.
479 The calculation of the integration time (Lal, 1991), a most conservative minimum age
480 estimate of terraces is described in Supplementary Section 4.1.1.
481
482 Aiming at an age estimate of the studied terraces, χ^2 minimizations were performed using a
483 modified version of the *^{10}Be profile simulator 1.2* of Hidy et al. (2010) for profiles where the
484 ^{10}Be concentrations showed the expected exponential decrease with depth. After preliminary
485 quick tests, user defined χ^2 cut-off values were defined for each dataset to provide 100 000
486 model solutions for each simulation, and fulfill the Bayesian statistics. The applied Monte
487 Carlo simulation parameters are presented in Table 3 and are described in the Supplementary
488 Section 4.1.2.
489 Results presented in this paper are based on Bayesian probability density functions (PDF)
490 of the *depth profile simulator*. The Bayesian 1σ and 2σ upper and lower values (Table 4)
491 represent the uncertainty of the simulation results, thus were used to calculate the relevant
492 error bars. Bayesian 2σ lower ages are taken as minimum ages when ^{10}Be concentrations are
493 in secular equilibrium. This approach leaves only 2.5% probability of a lower age estimate.
494 This was the case for Grébics, Bana and Győr locations. For the Mocsa site, where ^{10}Be
495 concentrations have not reached a secular equilibrium yet, the reported uncertainties are
496 Bayesian 1σ lower and upper values. For denudation rate and inheritance the Bayesian most
497 probable values with a 1σ confidence level are discussed.

At the Ács site the alluvial sediments had a cover of aeolian origin with no exponential decrease of the TCN concentrations. Here a different approach has been applied, which is described later.

Complete data tables of the simulator results and statistics are found in table S4.

4.2. Exposure age – denudation rate determination of the terrace IV

Three sample sites, Győr, Bana and Grébics belong to this horizon. According to field evidences, considerable thickness of fluvial material has been eroded from the tIV terrace. Fine overbank deposits, which are usually deposited on top of glacial terraces (Bridgland, 2000) are usually missing from the terrace surface. Borehole data from both the actual floodplain and from terraces in the neighbouring Gerecse Hills, where freshwater limestone locally protected the complete alluvial sequence, suggest that several meters of overbank sediments on top of the coarse material was typical along the Danube. Based on these evidences, a minimum total denudation of 5 m for the lower, more extended terrace remnants (Győr, Bana, Figs. 2A, 3) and 6 m for the highest, most eroded location (Grébics, Figs. 2A, 3) was constrained during the simulations to get the most probable minimum ages. The upper threshold of total denudation was set as high as 15 m and 16 m, respectively. The upper and lower age limits for the simulations were determined using stratigraphical and paleonthological evidences (described in Section 2.2) (Fig 4, Table 3).

The **Győr profile** (Dan08-02 to -12, Table 2) is the only one where sand and amalgamated pebble sub-samples could be separated by sieving and were processed separately, as there was enough material from both grain sizes to have a sample set of at least five samples, the minimum sample number for depth profile modelling (Hidy et al., 2010).

The ^{10}Be concentrations resulted to be consistently slightly higher in sand than in pebble sub-samples, with both showing an exponential decrease towards depth (Table 2, Fig. 7A). The variable inherited TCN concentrations of individual pebble samples was described by several authors (e.g. Schmidt et al., 2011; Codilean et al., 2014), however this effect can be overcome by sampling along depth profiles and using amalgamated pebble and/or sand samples (Anderson et al., 1996); the approach followed by this study. Aguilar et al. (2014) suggested that different denudation processes on the catchment and the effect of size reduction of larger boulders may be responsible for the smaller ^{10}Be concentrations in alluvial gravel than sand in a semi-arid catchment of the central Andes. On the other hand, several

532 authors described a positive correlation between grain size and ^{10}Be concentrations (Schmidt
533 et al, 2011), while others reported variable or similar TCN concentrations in different grain
534 sizes (Schaller et al., 2001; for a revision refer to Carretier et al., 2015). The discussion of
535 catchment-scale denudation processes of the Danube River is out of the scope of this study
536 due to the size and complexity of the drainage area.

537 The observed exponential decrease of ^{10}Be concentrations with depth for both pebble and
538 sand suggest that the inherited ^{10}Be inventory is constant along the profile, although at
539 different concentrations for pebble and sand samples. Therefore, the post-depositional
540 exposure history can be modelled using TCN concentrations of each grain size fraction (Hidy
541 et al., 2010). Both models are expected to provide similar exposure age – denudation rate
542 pairs, but with a different amount inherited ^{10}Be concentration.

543 Profile simulations (*depth profile simulator* of Hidy et al., 2010) were performed
544 separately for the sand and for the pebble profiles. Simulation settings were similar (Table 3)
545 as they share the same post-depositional exposure history. A wide user defined range of
546 inheritance was chosen to cover the expected values for both the sand and the pebble profiles.
547 The user defined χ^2 cut-off value was much lower for the pebble profile than for the sand (2
548 and 15, respectively), suggesting a better model fit of the pebble profile (n=5) then for the
549 sand profile (n=8).

550 Considering all sand samples the simulator was not able to find a solution because of the
551 distinctly low ^{10}Be concentration of the bottom samples (Dan08-11 and-12; Table 2, Fig. 7A).
552 These samples represent a cross-bedded sand layer underlying the coarser, graded channel
553 deposits of the upper 4.3 meters of the profile and showed sharply different maximum
554 denudation rate values (Figs. 5A, 6A, Table 2). The measured ^{10}Be concentrations suggest
555 that this sand unit originates from a previous sedimentation phase. Therefore, samples #11
556 and #12 were excluded from further simulations.

557 The simulation results approved that the ^{10}Be concentrations have reached secular
558 equilibrium (Figs. S1A, S2A, Table S4). Bayesian 2σ lower ^{10}Be exposure age of the Győr
559 profile is >693 ka for the pebble and >708 ka for the sand profile, suggesting a minimum
560 exposure age of the terrace around >700 ka (Table 4) for this site.

561 Probability density functions (PDF) are similar for pebble and sand (Fig. S1A). They show
562 well determined peaks for denudation rate ($6.5^{+1.6}_{-0.7}$ m/Ma and $7.0^{+0.5}_{-1.2}$ m/Ma for pebble and
563 sand) with values in agreement within error with each other and with the previously
564 calculated maximum denudation rate (Table 4). The inherited ^{10}Be component resulted to be

lower for the pebbles than for the sand (70^{+14}_{-5} kat/g and 95^{+27}_{-12} kat/g, respectively), as it was expected (Table 4, Fig. 7A).

From the sample set at **Bana** (Dan08-20 to-26) the Dan 08-22 sample had considerably higher ^{10}Be concentration than suggested by its subsurface depth (Table 2, Fig 7B), therefore it was excluded from depth profile modelling as an outlier. The previously suggested steady state ^{10}Be concentrations were confirmed by the depth profile modelling (Figs. S1B, S2B, Table S4). Monte Carlo simulations yielded a Bayesian 2σ lower exposure age of >477 ka with a well constrained most probable denudation rate of $10.0^{+0.2}_{-0.1}$ m/Ma and inheritance of 106^{+35}_{-14} kat/g (Table 4).

.The ^{10}Be concentrations of the top samples of the **Grébics** profile (Dan08-40 and -41) suggested that the upper 50 cm could be mixed during quarrying (Table 2, Figs. 5C, 6C). Accordingly, the arithmetic mean of the ^{10}Be concentrations of the two upper samples was placed in their average depth, in order to provide a rough estimate of ^{10}Be concentration relevant for the uppermost part of the profile (Fig. 7C). This *Dan08-40-41avg* sample was considered during the depth profile simulations.

The simulation results suggested also secular equilibrium of ^{10}Be concentrations (Figs. S1C, S2C, Table S4). The Bayesian 2σ lower exposure age of the Grébics profile resulted to be >659 ka; with a well determined denudation rate of $8.7^{+1.2}_{-0.8}$ m/Ma and an inheritance of 85^{+24}_{-16} kat/g (Table 4).

4.3. Exposure age – denudation rate determination of the terrace IIb

At **Mocsa** (Dan08-31 to -35) the sandy gravel channel facies of the terrace was covered by fine overbank sediments in 1.3 m thickness. Therefore, ^{10}Be samples were taken from the 1.3 to 4 meter depth range (Figs. 5D/1, 6D/1, 7).

For the depth profile modelling, user defined lower and upper age thresholds were determined as 14 and 360 ka, respectively (Table 3), on the basis of geological, stratigraphical and paleontological data integrated by the revision of the terrace chronology (Fig. 4). Total amount of eroded material was maximised at 500 cm, due to the presence of the overbank fine sediments and low position of the terrace.

598 Simulation results are presented by Figs S1D, S2D, Table S4. The Bayesian most probable
599 age of the terrace at Mocsa was 149^{+160}_{-13} ka, with an associated denudation rate of $5.8^{-2.1}_{+2.6}$
600 m/Ma and an inherited ^{10}Be concentration of 91^{+4}_{-4} kat/g (Table 4). As a result of the lack of
601 uppermost part of the depth profile, the exposure age could be constrained only with large
602 uncertainty towards older ages.
603
604 At **Ács** the measured ^{10}Be concentrations were significantly higher in the sandy gravel of
605 fluvial origin than in the aeolian cover sediments. The measured ^{10}Be concentrations did not
606 display the expected exponential decrease with depth (Table 2, Fig. 7E). The mean ^{10}Be
607 concentration of the cover (84±8 kat/g) is similar (within error) to that of the actual Danube
608 gravel (Dan08-27; Table 2) and to the mean inheritance signal of the other profiles.
609 The lack of exponential decrease in the cover may suggest (1) vertical sediment mixing in
610 the upper 130 cm, (2) dominance of the inherited component due to the very young age of the
611 sediment or (3) recent truncation of the upper part of the profile (at least 3 m material stripped
612 off).
613 The possibility of mixing (1) could not be excluded due to the proximity of the present day
614 soil, and the presence of recent biogalleries (Fig. 5E). The recent deposition of the loess with
615 a constant inherited ^{10}Be concentration (2) is improbable as the youngest published OSL age
616 of fine-sandy loess was 14±2 ka (Thamó-Bozsó et al., 2010) and in the Pannonian Basin all
617 data suggest that loess formation ceased during the Holocene. The likelihood of recent
618 truncation of several meters of material (3) from the top of the terrace surface seems to be
619 limited due to the low position and flat topography of the terrace and also due to the
620 conservative denudation rates calculated for all terraces, including those at higher positions
621 (Table 4). The surface of this terrace segment is hummocky, with variable depth of wind-
622 blown material. Therefore, wind erosion and formation of deflation hollows may have
623 occurred.
624 In the lower, fluvial part of the profile, ^{10}Be concentrations are roughly constant near 130
625 kat/g. A slight decreasing trend with depth can be observed only in the upper 60 cm (samples
626 Dan13-11 – 13; Table 2). Field observations (Supplementary Section 3.1.5 and Figs. 5E, 6E)
627 suggest that considerable cryoturbation affected the fluvial sediment at this site. The lack of
628 exponential decrease and the high ^{10}Be concentrations (significantly above the inheritance of
629 the other terraces and the actual Danube gravel; Tables 2, 6) suggest that periglacial mixing
630 might have affected the entire profile.
631 To simulate this profile, two models can be proposed:

1) In a simplistic two-step approach in step one, the lower part of the profile is deposited with an important inheritance signature; after short exposition, this deposit was covered by fine material. This scenario yields to an age of ~4ka for the fluvial terrace abandonment with an inherited concentration of 124 kat/g and a present fine deposition event with inherited ^{10}Be concentrations of ~83 kat/g. This scenario can be excluded due to the position of the terrace 12 m above the river, to the time needed for the development of the reddish paleosoil on top of the terrace material and also due the cryoturbation and loess formation on top of the terrace material, both requiring periglacial and/or arid climate conditions (in contrast with the present day temperate climate of the area).

2) After sedimentation, the alluvial material was exposed and a reddish paleosoil developed on its top. Soil formation was stopped by climate deterioration, and the sequence was mixed under periglacial conditions. This event erased the former exponential decrease of ^{10}Be concentrations with depth. Cryoturbation was followed by loess deposition.

Accepting this latter scenario, it was possible to assess the duration of buried exposure time of the alluvium using the slight exponential decrease of ^{10}Be concentrations in the upper part of the fluvial sediments. Simulation settings appear in Table 3, results are presented in Table 4, Fig. S1E, S2E. The user defined denudation rate was between 0 and 10 m/Ma, based on denudation rate data obtained from the other sample locations (Table 4). Our tentative age estimate for the age of loess deposition (buried exposure of the terrace) is 12^{+26}_{-6} ka.

4.4. Luminescence characteristics of the samples, post-IR IRSL ages

4.4.1 Dose-recovery, residuals, fading

The D_e values for the pIRIR signals are obtained by integrating the first 2.5 s of the IRSL decay curve and the final 100 s of the stimulation is subtracted in order to remove the background. Dose response curves were fitted using single or double exponential function (Fig. 8A,B). For all experiments only aliquots with a recycling ratio consistent with unity ±10 % and with a recuperation < 10% were accepted.

Prior to the equivalent dose measurements dose-recovery tests were carried out on one sample from each profile to test the reliability of the applied measurement protocol. The aliquots were bleached in a Hönle solar simulator for three hours. Dose-recovery ratios range between 0.94±0.04 and 1.15±0.05. These values – except the sample from Mocsa, which has

the highest dose-recovery ratio (1.15±0.05) – are surprisingly low. Other authors reported higher dose-recovery values (often >1.1) (Stevens et al., 2011; Thiel et al, 2011, 2014; Schatz et al., 2012). Murray et al (2014) compared the dose-recovery values after bleaching in solar simulator or window (sunlight bleaching) and concluded, that the bleaching in solar simulator results in better dose-recovery ratios. In our case the reason for the unexpectedly good dose-recovery ratios is probably the same.

Residual signals were also measured after sunlight bleaching in window and a small residual signal (<2Gy) was only observed for the samples. This residual dose was not subtracted either from the recovered dose, or from the natural dose estimates because this can be considered negligible.

Fading tests were carried out on six samples (4-8 aliquots), one from each profile at Bana and Mocsa and on all samples from the profile at Ács. The fading rates (g-values) are shown in Table S5. Large inter- and intra-sample variation was observed. The fading measurements resulted in very large scatter in g-values and sometimes negative g-values, probably as laboratory measurement artefacts. However, our observation is not unique, many authors have reported about negative or even anomalously high g-values in some cases (Murray et al., 2014; Trauerstein et al., 2014; Lowick et al., 2012). Our results range between -4.35±2.54 and 4.56±2.36 %/decade (Table S5), and some of them are much higher than those reported in other studies (<1-1.5%/decade) (Thiel et al., 2011, 2014; Murray et al., 2014; Schatz et al., 2012). This difference might be explained by mineral and grain-size differences (polymineral fine grained versus coarse-grained K-feldspar samples). The detected large scatter of the fading rates indicates that the measured values are probably unreliable for our samples. (However, averaging our measured fading rates resulted in g-value of 1.5+/-1.2%/decade (Table S5), which can be acceptable for the pIRIR-290 signal.) Nevertheless, it has already been demonstrated by previous studies (Thiel et al., 2011; Buylaert et al., 2012) that the pIRIR-290 signal is stable, not influenced by anomalous fading (Wintle, 1973) (e.g.: natural pIRIR-290 signal is consistent with saturation), therefore we did not correct the ages for fading at all.

4.4.2 Equivalent dose, incomplete bleaching, saturation, age estimates

D_e values range from 46.2±3.2 Gy to 386.8±9.5 Gy (Table 5). The pIRIR-290 signal has not reached the saturation level for five samples (Mocsa-1, -2, Ács-A1, -A2, -A4) (Figs. 5D,E, 8A,B). These D_e values correspond to age estimates from 15.2±1.3 ka to 146±10 ka.

Representative shine-down and dose-response curves from Mocsa-2 and Ács-A2 are shown in Fig.8 A,B.

Considering the fluvial origin of the samples, we can expect partially bleached minerals, which would result in age overestimation (Rodnight et al., 2006). Therefore, we applied small aliquots (10-30 grains/aliquot) for the measurements, which are more or less able to mimic the single grain measurements. We found that all of our samples (which were not in saturation) resulted in D_e distributions almost within ± 2 sigma. Radial plots of the small aliquots (Fig. 9) do not show wide De distributions therefore severe incomplete bleaching can be excluded for the samples. Although, as Reimann et al. (2012) and Trauerstein et al. (2014) reported, signal averaging can still be detected in case of small aliquots compared to single grain dating, but this might be more emphatic for young samples. In this study the fading corrected results of the pIRIR-225 protocol (Table S6) show good agreement with the pIRIR-290 ages (Table 5), which indicates that our samples are not influenced by severe incomplete bleaching as the pIRIR-225 signal is easier bleachable than the pIRIR-290 signal. The results of the pIRIR-225 measurement protocol are described in the Supplementary Section 4.4.3. Nevertheless, in case we failed to detect the effect of incomplete bleaching, the residual dose measured on a modern fluvial sample (Trauerstein et al., 2014) would correspond to a potential pIRIR-290 age overestimation of about 13.5 ka, which is about 10% of the age of our fluvial samples. The residual signal would be significant for younger samples when the magnitude of the residual dose is similar to the natural dose. Therefore the mean age was calculated to estimate the pIRIR ages.

The pIRIR-290 signal was observed in saturation for four samples out of nine (Bana-A1, -A2, -B3, Ács-B3) (Fig.8C). The ratio of the sensitivity-corrected natural signal to the laboratory saturation level was calculated for these samples and they ranged from 0.87 to 0.95 (Table 5). Therefore only minimum equivalent doses and age estimates were calculated for these samples (Wintle and Murray, 2006; Murray et al., 2014) (a single exponential growth curve was fitted to the data points and the $2*D_0$ value was calculated to assess minimum age estimates). These minimum dose estimates scatter around 1000 Gy, range from 904 Gy to 1120 Gy similarly as it is reported by Murray et al. (2014). They suggest that finite dose estimates cannot be used beyond ~1000 Gy, which results in age estimate around 300 ka considering a dose-rate of 3-4 Gy/ka for fine-grained sediment. In this study the total dose rates are lower, ranging from 2.26±0.21 Gy/ka to 3.51±0.17 Gy/ka (Table 5) therefore age estimates up to 400 ka are possible.

All three samples from the Bana profile (tIV, Figs. 5B, 6B) were beyond the datable time range because the pIRIR-290 signals were already in saturation (Fig. 8C). Therefore only minimum ages were estimated from this profile, >410 ka for sample Bana-A1, >386 ka for sample Bana-A2 and >320 ka for sample Bana- B3 (from the underlying late Miocene sand) (Table 5). As the uppermost sample yielded the oldest minimum age, the entire profile can be considered as >410 ka, which is in accordance the ^{10}Be exposure age estimate of this terrace (Table 6).

Two sand samples from the tIIb terrace at Mocsa (Figs. 5D/2, 6D/2) provided age estimates of 139±9 and 146±10 ka for the sediment burial (Table 5), which are in agreement with our ^{10}Be exposure age estimate (Table 6).

Four samples were collected from the terrace profile at Ács (Figs. 5E, 6E). The sample Ács-B3 was taken from the material underlying the terrace and it approaches saturation, therefore a minimum age of >258 ka was determined for this sample (Table 5). The fluvial terrace material, samples Ács-A2 and Ács-A4 provided age estimates of 95±6ka and 86±6 ka, respectively. Accumulation of the aeolian cover of the terrace was dated to 15±1 ka, which is similar to the buried exposure time estimated for the fluvial sediments (Table 4).

5. Discussion

Both post-IR IRSL and TCN dating methods were successfully applied to determine the age of deposition of Danube terraces. For the older terraces only minimum ages could be assessed by both methods. For the higher terrace remnants (tIV) the depth profile modelling of ^{10}Be data using the *^{10}Be depth profile simulator* (Hidy et al., 2010) allowed determining older minimum terrace ages compared to luminescence dating at one location (Bana; Table 6). Consequently, no further post-IR IRSL samples were processed from this horizon. On the other hand, for the lower/younger horizons the post-IR IRSL method provided better constrained terrace ages. The combination of the two methods enabled a more robust age determination than using either method separately (Guralnik et al., 2011).

5.1. Early Pleistocene age of the terrace IV of the study area

Accurate dating of the tIV terraces was difficult due to secular equilibrium of ^{10}Be concentrations and saturation of the luminescence signal. Nevertheless, ^{10}Be minimum ages

from >477 to >708 ka and a post-IR IRSL minimum age of >410 ka could be determined for this horizon (Table 6). ^{10}Be depth profile modelling enabled the determination of the oldest minimum terrace age at Győr due to the lowest denudation rate at this location (Tables 4, 6). Accordingly, we consider the >700 ka ^{10}Be exposure age as the best estimate for the entire tIV terrace range, which is concordant with the other minimum ages younger than >700 ka. This age is considerably older than the ~420 ka age of terrace abandonment suggested by the revised traditional terrace chronology (Fig. 4) and is well in agreement with the 540-2600 ka age range provided by malacological investigations of Krolopp (1995).The >700 ka minimum age of the highest terrace flight of the GTT is comparable with the estimated age of the tV or tVI horizon of the TR (Figs. 3, 4). As the tVI horizon is considered to be the first Danubian terrace in the TR marking the beginning of river incision in the Hungarian Danube valley, we propose that the highest terrace of our study area (tIV) may share the same age as tVI in the TR. Consequently, in the following part of this study we use the name tIV-VI for this terrace.

On the other hand, our results do not support the proposed link between terrace formation and MIS terminations (Gábris 2008, Gábris et al., 2012; Fig. 4) during the middle Pleistocene. Interestingly, we did not find any evidence on the existence of terrace horizons between 143±10 ka and >700 ka in the study area. Middle and late Pleistocene times are usually represented by at least 4-5 terraces in Europe (Gibbard and Lewin, 2009 and references therein) and in the TR (Pécsi, 1959; Ruszkiczay-Rüdiger et al, 2005a, Gábris and Nádor, 2007; Gábris et al, 2012), with well-expressed horizons usually linked to the Mindel glacial (MIS 12). We propose that these horizons may have also developed in the study area, but were most probably destroyed by the subsequent lateral erosion of the Danube. The uplifting barrier of the TR composed of more resistant lithology could lead to an increased sinuosity (and thus severe lateral erosion) of the Danube in the study area (Schumm et al., 2002), situated just upstream of the TR (Figs. 1, 3)

5.2. Separation of the late Riss/Saale (tIIIa) and Early Würm/Weichsel (tIIb) terraces

It was in question whether all the terrace remnants considered formerly as tIIb (with elevations 12-16 m and 17-22 m above the Danube) belonged to the same level sharing the same age, as suggested by Pécsi (1959). Mapping of the base of the Quaternary sediments (using shallow borehole data; Kaiser, 2005) revealed a 6-8 m high riser between the base of

800 the lower and higher parts of this terrace, suggesting the existence of two separate terrace
801 horizons, whose surface scarp was usually masked by erosional processes.
802 Post-IR IRSL dating provided well constrained burial ages of 139±9 and 146±10 ka
803 (averaging at 143±10) for the Mocsa site (20m amrl; Tables 5, 6). Cosmogenic in situ ^{10}Be
804 dating provided 149^{+160}_{-13} ka exposure age, coinciding within error with IRSL results both
805 suggesting terrace deposition during MIS 6 (130-190 ka; Lisiecki and Raymo, 2005). The
806 luminescence age of 95±6 ka and 86±6 ka (averaging at 91±6) of the terrace at Ács (12m
807 amrl) proposes an early Würmian (MIS 5b-c) age of this terrace.
808 Considering the elevation and the age differences of the Mocsa and Ács locations (Table
809 6), we propose the separation of these terraces. We suggest that a higher level has developed
810 during the late Riss glacial (MIS 6; Mocsa), which we index as tIIIa (after Gábris and Nádor,
811 2007) and that the lower, tIIb level has formed during the early Würm glaciation (MIS 4-5;
812 Ács) (Fig. 4).
813
814 *5.3. Climate control on the onset of terrace formation*
815
816 Our new chronological data suggests that MIS based terrace chronology proposed by
817 Gábris (2008) is reasonable for the low terraces up to tIIIa, but it is not applicable for the
818 higher terraces (Fig. 4). Apparently, during the middle Pleistocene not all the climate
819 fluctuations led to terrace formation or these terraces were destroyed later by the river.
820 The first major worldwide Pleistocene glacial events with substantial ice volumes in
821 continental areas outside the polar regions occurred around 0.8-0.9 Ma (MIS 22) (Ehlers and
822 Gibbard, 2007; Clark et al., 2006; Gibbard and Lewin, 2009). After the "mid-Pleistocene
823 climate transition" (Clark et al., 2006; ca. 1.2-0.7 Ma) dominantly cold climate conditions
824 with short episodes of glaciations and brief interglacials prevailed. The >700 ka minimum age
825 of the uppermost, tIV-VI horizon in our study area is reconciliable with a river style change
826 triggered by the "mid-Pleistocene climate-transition" when mechanism of larger rivers in
827 Western Europe shifted from valley widening to incision (Gibbard and Lewin, 2009). Burial
828 age determination of cave sediments in the northern Swiss Alps revealed an abrupt increase of
829 valley incision rates (from 0.12 mm/a to 1.2 mm/a) at 0.8-1.0 Ma (Häuselmann et al., 2007a),
830 in good agreement with the time of the mid-Pleistocene climate transition.
831 Hence, we suggest that abandonment of the former wide valley and onset of incision may
832 have started in connection with this climate event as a complex response of the river to the
833 propagation of the compression related vertical movements from the SW towards the basin

interior and of climate change. Accordingly, the minimum age of >700 ka of the highest terraces may be valid for the Hungarian Danube valley as the onset valley incision, instead of the Plio-Pleistocene boundary, suggested by Pécsi (1959).

Resolution of our data does not enable the distinction between climatically or tectonically triggered terrace formation. Fold related uplift of the TR and subsidence of the neighbouring lowlands (Figs. 1, 3) necessarily led to river incision in and around the uplifting TR, where terraces were formed as a consequence of the interplay (positive and negative feedbacks) between the ongoing uplift and climate change.

5.4. Denudation of the terrace surfaces

Multielectrode resistivity profiles (MUEL; Fig. 10) and field experiences demonstrate that the tIV-VI horizon is represented by a sheet of coarse-grained material in up to 8-10 m thickness, which is underlain by fine sand (of late Miocene age; Magyar et al., 2007, 2013). It is also well visible, that the base of the terrace remnant at Bana is around 150 m asl. (Fig. 10A,B) and goes as high as ~185 m in the eastern termination of the GTT (Fig. 10D,C). Decreasing thickness of the gravel sheet towards the margins of the terrace remnant hills is indicative of more intensive denudation towards the terrace scarps. It is also visible that coarse terrace material is thinner at the eastern, higher section of the GTT, where their maximum apparent thickness is 3-5 m (Geomega, 2004).

Cosmogenic ^{10}Be depth profiles provided well constrained denudation rates of the terrace surfaces (Table 6). The highest denudation rates were calculated at Bana $10.0^{+1.1}_{-0.6}$ m/Ma) and at Grébics ($8.7^{+1.2}_{-0.8}$ m/Ma), at the edge of the terrace remnant and on the small, isolated terrace hill at the most elevated part of the terrace region, respectively. Lower denudation rate was detected on larger flat surfaces: $6.5^{+1.6}_{-0.7}$ m/Ma and $7.0^{+0.5}_{-1.2}$ at Győr and $5.8^{-2.1}_{+2.6}$ m/Ma at Mocsa. Considering the minimum exposure ages of the terraces these rates suggest 5-8 m of material eroded from the tIV-VI terraces and ~1.0 m denudation from the tIIb-tIIIa at Mocsa.

The raw calculations of maximum denudation rate (Table 2) provided slightly lower values than denudation rates provided by the *depth profile simulator* (Hidy et al., 2010). This is because during depth profile simulations the inherited amount of ^{10}Be is considered and density is a free parameter between 1.8 and 2.2 g/cm^3. On the other hand, when maximum denudation rate is calculated for each sample (Table 2), it is not possible to account for the inheritance and density is a fixed value (at 2 g/cm^3).

867 Portenga and Bierman (2011) reported that basin-averaged ^{10}Be denudation rates are
868 usually faster than outcrop erosion. In their study mean and median basin-averaged
869 denudation rates in the temperate climate zone were 277 m/Ma and 84 m/Ma, while for
870 outcrops these were 25 m/Ma and 16 m/Ma, respectively. The difference between the 30-80
871 m/Ma typical basin-averaged ^{10}Be denudation rates of middle European rivers (Schaller et al.,
872 2002) and low (up to 10 m/Ma) rates of terrace denudation in the GTT of this study suggest
873 increasing relief of the study area, as it is expected by the river incision and terrace formation
874 described in the area. Coarse grained fluvial material have protected the high terraces from
875 surface denudation, which led to surface inversion: the former riverbed has now the highest
876 topography of the area. Due to their slow denudation, these terraces serve as appropriate tools
877 to reconstruct former stages of valley evolution and thus to quantify valley incision and
878 tectonic uplift (see in section 5.6).
879
880 *5.5. Cryoturbation features*
881
882 The periglacial involutions in the outcrop at Ács were observed down to a depth of 1-1.5 m
883 from the top of the alluvial material, with no signs of mixing in the aeolian cover (Figs. 5E,
884 6E). Periglacial sedimentary features were frequently observed in the western Pannonian
885 Basin (Pécsi, 1961, 1997; Van Vliet-Lanoë et al., 2004). Their development was attributed to
886 glacial periods of the Würm and/or Riss glaciations and possibly in earlier glacial phases, at
887 locations where local climate and soil conditions were suitable for cryoturbation (e.g.
888 Matsuoka, 2011; Ruszkiczay-Rüdiger and Kern, 2015).
889 Our sampling occurred outside these well visible signs of sediment mixing (Figs. 5E, 6E).
890 However, the lack of exponential decrease of the measured ^{10}Be concentrations suggests that
891 cryoturbation affected the former terrace, even outside the involutions and at least down to a
892 depth of 3 m (Table 2, Fig. 7).
893 The post-IR IRSL age of the terrace sedimentation was 91±6 ka and the age of loessy-fine-
894 sand cover proved to be 15±1 ka (Table 6). The latter age is similar to the youngest age of
895 loess formation in the region (Thamó-Bozsó et al, 2010) during the latest Pleistocene (end of
896 MIS 2). The ^{10}Be exposure age estimate (covered exposure time of the alluvial sediments) of
897 12^{+26}_{-6} ka of the cover, is in agreement with its post-IR IRSL age.
898 These ages are bracketing the development of a 30-40 cm thick reddish-brown paleosoil
899 developed on top of the alluvial sediments, which was subsequently deformed by the
900 cryoturbation before the deposition of the aeolian cover. The post-IR IRSL dated loess-

paleosoil sequence of the Süttő quarry in neighbouring Gerecse Hills showed that several paleosoil horizons were formed between ~85 and ~30 ka, with the most prominent one during the MIS 3 (Novothny et al, 2011). Accordingly, the formation of the paleosoil on the alluvial sediments at Ács during this period is highly probable, which could be affected by cryoturbation under the periglacial climate conditions of MIS 2 (Ruszkiczay-Rüdiger and Kern, 2015).

5.6. Incision rates and tectonic uplift

Uplift of the TR was related to the neotectonic shortening and related large-scale folding of the Pannonian lithosphere (Horváth and Royden, 1981, Horváth et al. 2015), which progressively shifted from SW (Slovenia) toward NE (Tari, 1994; Fodor et al. 2005). The >700 ka minimum age of the highest terraces of the area put forward that the onset of uplift in the northeastern part of the TR started before this time, but probably somewhat later than in the southwest TR (Fig.1), where the minimum age of the onset of the uplift was 1.56±0.09 Ma, as determined by in situ ^{10}Be exposure age of wind-abraded landforms (Ruszkiczay-Rüdiger et al., 2011).

The maximum incision/uplift rates relevant for the minimum age of the IV-VI terrace level (>700 ka) were calculated. Elevation of the terraces was corrected for the material thickness eroded from their surface since their abandonment by the river (calculated using ^{10}Be denudation rates, Table 6, Section 5.4). The maximum incision rates show a positive correlation with the elevation of the terrace remnants with values from <0.06 mm/a to <0.13 mm/a (Győr: <0.06 mm/a; Bana: <0.07 mm/a; Grébics: <0.13 mm/a) (Fig. 11, Table S7). The increase of incision rates from west to east along the Danube reflects well the trend towards higher uplift rates closer to the uplifting TR (Figs. 1, 3). These rates are half of the maximum rates calculated based on the revised traditional chronology (Fig. 11) and are in the same order of magnitude as incision/uplift rates revealed by former studies in Europe (Table 1).

For the young terraces, incision rates of 0.15±0.01 mm/a (Mocsa) and 0.13±0.01 mm/a (Ács) were computed using the post-IR IRSL data. Our results suggest somewhat faster uplift rates for the young terraces (Mocsa, Ács) than for the tIV-VI terraces at the same position along the river (Fig. 11). This might indicate slight acceleration of uplift towards present, which would be in accord with the gradual built-up of compressional stress-field in the Pannonian Basin resulting in an increasing trend of vertical movements (Bada et al., 2006).

However further data are necessary to decide whether our data indicates a true acceleration of vertical movements.

Proposing that the abandonment of the highest terrace level of the Hungarian Danube valley was triggered by the same tectonic and climatic processes, we tentatively extrapolated the >700 ka minimum age to the highest terraces of the valley across TR and calculated the uplift rates for each valley segment (blue dotted line on Fig. 11, Table S7). The comparison of the uplift rates along the Danube calculated using our minimum age estimate of >700 ka and the uplift rates calculated on the basis of the quantification of the traditional terrace chronological data (orange line of Fig. 11) it is visible, that while in the GTT the traditional data suggest considerably higher values, within the TR the maximum uplift rates are similar, with <0.36 mm/a and <0.33 mm/a at the axis of the TR (Danube Bend; Fig. 11). By the >700 ka based uplift curve (blue line and blue dotted line on Fig. 11) the anomalously high uplift rates suggested by the traditional terrace chronology for the eastern part of the GTT were eliminated, and the curve has a smooth continuation towards the TR.

A slight break can be suggested in the extrapolated uplift rate curve blue dotted line on Fig. 11), next to the locations of the travertine occurrences. As we noted earlier, there is a fault at the western margin of the Gerecse Hills, which was clearly active in the Late Miocene (Bartha et al. 2014). In case of Quaternary activity along this fault, the uplift rate may have changed at this fault. However, the spatial resolution of our quantitative data set is not dense enough to support or reject unequivocally the break in the curve (presence of active fault).

Uplift rates calculated using the time span determined by Th/U ages of travertines covering terrace surfaces (Kele, 2009; Kele et al., 2009, 2011; Sierralta et al., 2009) were 0.1-0.5 mm/a for the Gerecse and Buda Hills. The lower values of these estimates are in agreement with incision rates calculated in this study (Fig. 11, Table S7). We suggest that the higher incision rates were most probably derived from travertines deposited on the valley slope, i.e. not connected to the base level, thus providing excessively young ages relative to the abandonment of the dated terrace. Accordingly, we propose that for the quantification of valley incision and uplift rates the oldest travertine ages of a certain height are to be considered.

Th/U series dating of cave sediments in the Buda Hills (Szanyi et al., 2012) issued 0.15—0.32 mm/a uplift rate at the eastern margin of the TR; this is equally in agreement with our projected uplift rate values for the SE margin of the TR (Fig. 11, Table S7).

966 The maximum uplift rate estimated by this study for the Danube Bend is in accordance
967 with novel GPS velocity measurements suggesting that uplift rates in the axial zone of the TR
968 do not exceed 0.5 mm/a (Grenerczy et al., 2005, and oral communication 2014).
969 On the other hand, Ruszkiczay-Rüdiger et al. (2005b) measured very young ^{3}He minimum
970 exposure ages on the strath terraces of the Danube Bend and derived a maximum incision rate
971 of 1.6 mm/a. On the andesite strath surfaces terrace ages were estimated using surface
972 samples only. We suggest that the sampled strath surfaces were most probably affected by
973 significant denudation, which could not be accounted for using surface samples only. We
974 propose that ^{3}He concentrations of Ruszkiczay-Rüdiger et al. (2005b) may be better
975 interpreted as denudation rates providing 3-5 m/Ma denudation for the flat or gently dipping
976 strath surfaces (0-5°) and 16-17 m/Ma for the lowest horizon with a slope of 10° towards the
977 Danube, which values are reconcilable with denudation rates provided by the depth profiles of
978 this study.
979
980
981 **6. Conclusions**
982
983 The combined application of TCN and post-IR IRSL technique on alluvial terraces can
984 lead to robust age determination. On old terraces TCN depth profile modelling provided better
985 age estimates (or minimum age) than luminescence, even if the site was affected by
986 considerable denudation. On the other hand, luminescence is not sensitive of sediment
987 mixing, high denudation rates or anthropogenic processes like stripping of the upper layers, as
988 long as the sediment is not brought to surface after its burial. Therefore, on locations affected
989 by any of these processes post-IR IRSL was a better approach, as long as sediment burial
990 occurred within its applicability range (300-400 ka).
991 Depth profile modelling of ^{10}Be concentrations of pebble and sand samples at Győr
992 provided similar exposure age - denudation rate pairs suggesting a terrace age of >700 ky and
993 a denudation rate of ~6.7 mm/a (Table 6). Accordingly, we suggest that both amalgamated
994 pebble and sand samples are suitable for age determination until the depth profile method is
995 used, because it allows considering their different amount of inherited ^{10}Be. For the highest
996 terrace flight of the study area (tIV-VI) this minimum age is considered as the best estimate
997 due to the lowest denudation rate calculated at this location. Besides, it is reconcilable with
998 the lower minimum ages of the other sample locations (Fig.4).

The >700 ka minimum age of terrace abandonment is considered as the lower time constraint of the onset of the valley incision in the northern part of the Pannonian Basin. Nevertheless, we emphasize that terraces were formed due to the complex effect of the propagation of fold-related vertical movements towards the basin interior and of climate change. The resolution of our data does not enable the differentiation between the effects of the two processes. However, we can safely conclude that the uplift of the northeastern TR started before 700 ka, and that the shift from the former wide valley to a narrower terraced valley may have been triggered by the mid-Pleistocene climate transition (0.7-1.2 ka; Clark et al., 2006), as it was recognised at several European rivers (Gibbard and Lewin, 2009).

We propose that the evolution of the Hungarian Danube valley was governed by the same tectonic and climatic processes, and that the highest terrace of the study area (tIV) shares the same age as the highest terrace horizon (tVI) of the TR. Accordingly, the >700 ka ^{10}Be minimum exposure age of the tIV-VI level of the GTT could be extrapolated to the subsequent valley sections. Maximum incision/uplift rates were calculated accordingly, and revealed <0.06-0.13 mm/a uplift rates increasing from west to east for the study area, and enabled an extrapolation suggesting the highest rate of <0.33 mm/a in the axial zone of the TR (Fig. 11, Table S7). These maximum rates show moderate tectonic deformation of the TR from the middle Pleistocene onwards. The rate of vertical deformation is in the same order of magnitude as published in other parts of Europe (Table 1).

Post-IR IRSL data at two locations on the former tIIb terrace enabled the differentiation of a higher horizon (20 m amrl) with an estimated age of 143±10 ka (Mocsa) and a lower horizon (12 m amrl) of 91±6 ka (Table 6). These results are the first geochronological evidences on the definition of the tIIb level of the Hungarian Danube valley as early Würm (MIS 5b-c), and to distinguish the higher, late Riss (MIS 6) terrace level as tIIIa. We could not find evidence on the existence of terrace remnants between <700 ka and ~143 ka in the GTT, therefore suggest that most of the terraces of middle Pleistocene times were possibly destroyed by the enhanced lateral erosion of the Danube.

Acknowledgements

Our research was supported by:

the OTKA PD83610, PD100315, K062478, K083150 and K106197.

the Research Scholarship of the French Embassy of Hungary,

the French-Hungarian Balaton-Tét Project (FR-32/2007; TÉT_11-2-2012-0005),
the EGT/Norvegian Financing Mechanism and MZFK (Zoltán Magyary Public Foundation of Higher Education), Hungary, and
the Bolyai János Scholarship of the Hungarian Academy of Sciences,
the "Lendület" program of the Hungarian Academy of Sciences (LP2012-27/2012).
The ^{10}Be measurements performed at the ASTER AMS national facility (CEREGE, Aix en Provence) were supported by the INSU/CNRS, the French Ministry of Research and Higher Education, IRD and CEA. The gamma-spectrometry measurements and part of the preparation of the luminescence samples were carried out at the Leibniz Institute for Applied Geophysics, Hannover, Germany. Special thanks to Christine Thiel, Jan-Pieter Buylaert and Andrew Murray for the fruitful discussions on post-IR IRSL results. Laetitia Leanni and Frederic Chauvet are acknowledged for their help during ^{10}Be chemistry. We are grateful for Gábor Bada, Prof. Frank Horváth and Bence Solymosi for providing their unpublished MUEL profiles of the GTT for this study.

References

Adamiec, G., Aitken, M. 1998. Dose rate conversion factors: update. Ancient TL 16, 37-50.

Aguilar, G., Carretier, S., Regard, V., Vassallo, R., Riquelme, R., Martinod, J., 2014. Grain size-dependent ^{10}Be concentrations in alluvial stream sediment of the Huasco Valley, a semi-arid Andes region. Quaternary Geochronology 19, 163-172.

Anders, M.D., Pederson, J.L., Rittenour, T.M., Sharp, W.D., Gosse, J.C., Karlstrom, K.E., Crossey, L.J., Goble, R.J., Stockli, L., Yang, G. 2005. Pleistocene geomorphology and geochronology of eastern Grand Canyon: linkages of landscape components during climate changes. Quaternary Science Reviews 24, 2428-2448.

Anderson, R.S., Repka, J.L., Dick, G.S. 1996. Explicit treatment of inheritance in dating depositional surfaces using in situ ^{10}Be and ^{26}Al. Geology 24, 47-51.

Antón, L., Rodés, A., De Vicente, G., Pallàs, R., Garcia-Castellanos, D., Stuart, F.M., Braucher, R., Bourlès, D. 2012. Quantification of fluvial incision in the Duero Basin (NW Iberia) from longitudinal profile analysis and terrestrial cosmogenic nuclide concentrations. Geomorphology 165–166, 50–61.

Arnold, M., Merchel, S., Bourlès, D.L., Braucher, R., Benedetti, L., Finkel, R.C., Aumaître, G., Gottdang, A., Klein, M., 2010. The French accelerator mass spectrometry facility

ASTER: improved performance and developments. Nuclear Instruments and Methods in Physics Research B 268, 1954–1959.

Bada, G., Horváth, F., Tóth, L., Fodor, L., Timár, G., Cloetingh, S., 2006. Societal aspects of ongoing deformation in the Pannonian region. In: Pinter, N., Grenerczy, Gy. (Eds.), The Adria Microplate: GPS Geodesy, Tectonics, and Hazards. NATO ARW Series. Kluwer Academic Publishers, 385-402.

Bada, G., Horváth, F., Dövéby, P., Szafián, P., Windhoffer, G., Cloetingh, S. 2007. Present-day stress field and tectonic inversion in the Pannonian basin. Global and Planetary Change 58, 165-180.

Balco, G., Briner, J., Finkel, R.C., Rayburn, J., Ridge, J.C., Schaefer, J.M., 2009. Regional beryllium-10 production rate calibration for late-glacial northeastern North America. Quaternary Geochronology 4, 93-107.

Bartha, I.R., Tőkés, L., Fodor, L., Csillag, G., Magyar, I., Lantos, Z., Sztanó, O. 2014.: Deltaic deposits and inundated basement blocks: consequences for paleotopography, Gerecse Hills, Hungary. Central European Meeting of Sedimentary Geology, Poster session, Olomouc, Czech Republic, Abstract Book, 13-15.

Bierman, P.R. 1994. Using in situ produced cosmogenic isotopes to estimate rates of landscape evolution: A review from the geomorphic perspective. J. Geophys. Res. 99/B7, 13885-13896.

Braucher, R., Brown, E.T., Bourlés, D.L., Colin, F. 2003. In situ produced ^{10}Be measurements at great depths: implications for production rates by fast muons. Earth and Planetary Science Letters 211, 251-258.

Braucher, R., Del Castillo, P., Siame, L., Hidy, A.J., Bourles, D.L. 2009. Determination of both exposure time and denudation rate from an in situ-produced ^{10}Be depth profile: A mathematical proof of uniqueness. Model sensitivity and applications to natural cases. Quaternary Geochronology 4, 56-64.

Braucher, R., Merchel, S., Borgomano, J., Bourles, D.L. 2011. Production of cosmogenic radionuclides at great depth: A multi element approach. Earth and Planetary Science Letters 309, 1-9.

Bridgland, D.R., 2000. River terrace systems in north-west Europe: an archive of environmental change, uplift and early human occupation. Quaternary Science Reviews 19, 1293–1303.

Bridgland, D., Westaway, R., 2008. Climatically controlled river terrace staircases: a worldwide Quaternary phenomenon. Geomorphology 98 (3–4), 285–315.

Briner, J.P., Young, N.E., Goehring, B.M., Schaefer, J.M., 2012. Constraining Holocene ^{10}Be production rates in Greenland. J. Quat. Sci. 27, 2-6.

Brocard, G.Y., van der Beek, P.A., Bourlés, D.L., Siame, L.L., Mugnier, J.L. 2003. Long-term fluvial incision rates and postglacial river relaxation time in the French Western Alps from ^{10}Be dating of alluvial terraces with assessment of inheritance, soil development and wind ablation effects. Earth and Planetary Science Letters 209, 197-214.

Buylaert J.-P., Jain, M., Murray, A.S., Thomsen, K.J., Jain, M. 2009. Testing the potential of an elevated temperature IRSL signal from K-feldspar. Radiation Measurements 44, 560-565.

Buylaert J.-P., Jain, M., Murray, A.S., Thomsen, K.J., Thiel, C., Sohbati, R., 2012. A robust feldspar luminescence dating method for Middle and Late Pleistocene sediments. Boreas 41, 435-451.

Carretier, S., Regard, V., Vassallo, R., Aguilar, G., Martinod, J., Riquelme, R., Christophoul, F., Charrier, R., Gayer., E., Farías, M., Audin., L., Lagane, C., 2015. Differences in ^{10}Be concentrations between river sand, gravel and pebbles along the western side of the central Andes. Quaternary Geochronology 27, 33-51.

Cerling, T. E., Craig, H. 1994. Geomorphology and in situ cosmogenic isotopes. Annu. Rev. Earth Planet. Sci. 22, 273-317.

Chmeleff, J., von Blanckenburg, F., Kossert, K., Jakob, J, 2009. Determination of the ^{10}Be half-life by multicollector ICP-MS and liquid scintillation counting. Nucl. Instr. and Meth. B. doi:10.1016/j.nimb.2009.09.012

Clark, P.U., Archer, D., Pollard, D., Blum, J.D., Rial, J.A., Brovkin, V., Mix, A.C., Pisias, N.G., Roy, M., 2006. The middle Pleistocene transition: characteristics, mechanisms, and implications for long-term changes in atmospheric pCO2. Quaternary Science Reviews 25, 3150–3184.

Codilean, A., Fenton, C., Fabel, D., Bishop, P., Xu, S., 2014. Discordance between cosmogenic nuclide concentrations in amalgamated sands and individual fluvial pebbles in an arid zone catchment. Quaternary Geochronology 19, 173-180.

Császár, G., Pistotnik, J., Pristas, J., Elecko, M., Konhcny, M., Vass, D., Vozár, J. 2000. Surface Geological Map. Danube Regional Environmantal Programme DANREG – Explanatory Notes. Jahrbuch der Geologischen Bundenstalt 142, 421-445.

DeLong, S.B., Arnold, L.J., 2007. Dating alluvial deposits with optically stimulated luminescence, AMS 14C, and cosmogenic techniques, western Transverse Ranges, California, USA. Quaternary Geochronology 2, 129–136.

1135 Dombrádi, E., Sokoutis, D., Bada, G., Cloetingh, S., Horváth, H. 2010. Modelling recent
1136 deformation of the Pannonian lithosphere: Lithospheric folding and tectonic topography.
1137 Tectonophysics 484, 1-4, 103-118.
1138 Dunai, T.J. 2010. Cosmogenic Nuclides. Principles, Concepts and Applications in the Earth
1139 Surface Sciences. Cambridge Univ Press, New York, 187 p.
1140 Ehlers, J. Gibbard, P. 2007. The extent and chronology of Cenozoic Global Glaciation.
1141 Quaternary International 164-165, 6-20.
1142 Fenton, C.R., Hermanns, R.L., Blikra, L.H., Kubik, P.W., Bryant, C., Niedermann, S.,
1143 Meixner, A., Goethals, M.M., 2011. Regional ^{10}Be production rate calibration for the past
1144 12 ka deduced from the radiocarbon-dated Grotlandsura and Russenes rock avalanches at
1145 69° N. Norway. Quaternary Geochronology 6, 437-452.
1146 Fodor L., Csontos L., Bada G., Györfi I., Benkovics L. 1999: Tertiary tectonic evolution of
1147 the Pannonian basin system and neighbouring orogens: a new synthesis of paleostress data.
1148 In: Durand, B., Jolivet, L., Horváth, F., Séranne, M. (eds.): The Mediterranean Basins:
1149 Tertiary extension within the Alpine Orogene. Blackwell Spec. Publ. Geol. Soc. London,
1150 156, 295-334.
1151 Fodor, L., Bada, G., Csillag, G., Horváth, E., Ruszkiczay-Rüdiger, Zs., Palotás, K., Síkhegyi,
1152 F., Timár, G., Cloetingh, S., Horváth, F. 2005. An outline of neotectonic structures and
1153 morphotectonics of the western and central Pannonian Basin. Tectonophysics 410, 15-41.
1154 Gábris, Gy. 1994. Pleistocene evolution of the Danube in the Carpathian Basin. Terra Nova 6,
1155 495-501.
1156 Gábris, Gy., 2008. Relation between the time scale of the river terrace formation and the
1157 Oxygen Isotope Stratigraphy in Hungary. In: Kertész, Á. & Kovács, Z. (eds): Dimensions
1158 and trends in Hungarian Geography. Studies in Geography in Hungary 33. Akadémiai
1159 Kiadó, Budapest, 19-31.
1160 Gábris, Gy., Nádor, A. 2007. Long-term fluvial archives in Hungary: response of the Danube
1161 and Tisza rivers to tectonic movements and climatic changes during the Quaternary: a
1162 review and new synthesis. Quaternary Science Reviews 26, 2758-2782.
1163 Gábris, Gy., Horváth, E., Novothny, Á., Ruszkiczay-Rüdiger, Zs. 2012. Fluvial and aeolian
1164 landscape evolution in Hungary – results of the last 20 years research. Geologie en
1165 Mijnbouw-Netherlands Journal of Geosciences, 91, ½, 111 – 128.
1166 Geomega 2004. Report for geophysical surveys on Danube terraces in Hungary. Unpublished
1167 research reposrt of the Geomega Ltd, Budapest, 14 p.

1168 Geyh, M.A. 2005. ^{14}C dating - still a challenge for users. Zeitschrift für Geomorph NF 139,
1169 63–86.
1170 Giachetta, E. Molin, P. Scotti, V.N. Faccenna, C. 2015. Plio-Quaternary uplift of the Iberian
1171 Chain (central-eastern Spain) from landscape evolution experiments and river profile
1172 modeling. Geomorphology 246, 48-67.
1173 Gibbard, P. and Van Kolfschoten, T., 2005. The Pleistocene and Holocene Epochs. In:
1174 Gradstein, F.H., Ogg, J.G. & Smith, A.G.: A Geologic Time Scale 2004. Cambridge Univ.
1175 Press, 441-452.
1176 Gibbard, P.L., Lewin, J., 2002. Climate and related controls on interglacial fluvial
1177 sedimentation in lowland Britain. Sedimentary Geology 151, 187–210.
1178 Gibbard, P.L., Lewin, J., 2009. River incision and terrace formation in the Late Cenozoic of
1179 Europe. Tectonophysics 474, 41–55.
1180 Goehring, B.M., Lohne, Ø.S., Mangerud, J., Svendsen, J.I., Gyllencreutz, R., Schaefer, J.,
1181 Finkel, R., 2012. Lateglacial and Holocene ^{10}Be production rates for western Norway. J.
1182 Quat. Sci. 27, 89-96.
1183 Gosse, J.C., Phillips F.M. 2001. Terrestrial in situ cosmogenic nuclides: theory and
1184 application. Quaternary Science Reviews 20, 1475-1560.
1185 Grenerczy, Gy., Sella, G., Stein, S., Kenyeres, A. 2005. Tectonic implications of the GPS
1186 velocity field in the northern Adriatic region, Geophysical Research Letters 32, L16311,
1187 doi:10.1029/2005GL022947.
1188 Guralnik, B., Matmon, A., Avni, Y., Porat, N., Fink, F. 2011. Constraining the evolution of
1189 river terraces with integrated OSL and cosmogenic nuclide data. Quaternary Geochronology
1190 6. 22-32.
1191 Hancock, G.S., Anderson, R.S., Chadwick, O.A., Finkel, R.C., 1999. Dating fluvial terraces
1192 with ^{10}Be and ^{26}Al profiles: application to the Wind River, Wyoming. Geomorphology 27,
1193 41–60.
1194 Häuselmann, P., Granger, D., Jeannin, P.Y., Lauritzen, S.E. 2007a. Abrupt glacial valley
1195 incision at 0.8 Ma dated from cave deposits in Switzerland. Geology 35. 143-146.
1196 Häuselmann, P., Fiebig, M., Kubik, P.W., Adrian, H., 2007b. A first attempt to date the
1197 original ‘‘Deckenschotter’’ of Penck and Brückner with cosmogenic nuclides. Quaternary
1198 International 164-165, 33-42.
1199 Hedrick, K., Owen, L.A., Rockwell, T.K., Meigs, A., Costa, C., Caffee, M.W, Masana, E.,
1200 Ahumada, E. 2013. Timing and nature of alluvial fan and strath terrace formation in the
1201 Eastern Precordillera of Argentina, Quaternary Science Reviews 80, 143-168.

1202 Hidy, A.J., Gosse, J.C., Pederson, J.L., Mattern, J.P., Finkel, R.C., 2010. A geologically
1203 constrained Monte Carlo approach to modeling exposure ages from profiles of cosmogenic
1204 nuclides: an example from Lees Ferry, Arizona. Geochemistry Geophysics Geosystems 11,
1205 Q0AA10. doi:10.1029/2010GC003084.
1206 Horváth, F. 1995. Phases of compression during the evolution of the Pannonian Basin and its
1207 bearing on hydrocarbon exploration. Marine and Petrol. Geol. 12/8, 837-844.
1208 Horváth, F., Musitz, B., Balázs, A., Végh, A., Uhrin, A., Nádor, A., Koroknai, B., Pap, N.,
1209 Tóth, T., Wórum, G. 2015. Evolution of the Pannonian basin and its geothermal resources.
1210 Geothermics 53, 328-352.
1211 Horváth, F., Royden, L. 1981. Mechanism for the formation of the Intra-Carpathian Basins: a
1212 Review. Earth Evolution Sci. 3, 307- 316.
1213 Horváth, F., Cloetingh, S. 1996. Stress-induced late stage subsidence anomalies in the
1214 Pannonian Basin. Tectonophysics 266, 287-300.
1215 Huntley, D.J., Baril, M.R., 1997. The K content of the K-feldspars being measured in optical
1216 dating or in thermoluminescence dating. Ancient TL 15, 11–13.
1217 Kaiser, M. 2005. Base of Quaternary sediments in the area of Komárom and Mocsa.
1218 Manuscript, Geological and Geophysical Institute of Hungary
1219 Kele, S. 2009. Investigation of travertines from the Carpathian Basin: paleoclimatological and
1220 sedimentological analysis (in Hungarian with English summary). PhD Thesis, Eötvös
1221 Univetsity, 176 p.
1222 Kele, S., Scheuer, Gy., Demény, A., Shen, C.-C., Chiang, H.W., 2009. U-series dating and
1223 isotope geochemical study of the Gellért Hill (Budapest) travertine. Central European
1224 Geology 52 (3–4), 199-224.
1225 Kele, S., Scheuer Gy, Demény A, Shen C.-C., Chiang H.-W., 2011. A Rózsadomb (Budapest)
1226 édesvízi mészköveinek U/Th sorozatos kormeghatározása és stabilizotóp-geokémiai
1227 vizsgálata. Földtani Közlöny 141 (2), 445–468.
1228 Korschinek, G., Bergmaier, A., Faestermann, T., Gerstmann, U.C., Knie, K., Rugel, G.,
1229 Wallner, A., Dillmann, I., Dollinger, G., von Gostomski, Lierse Ch., Kossert, K., Maitia,
1230 M., Poutivtsev, M., Remmert, A., 2009. A new value for the half-life of ^{10}Be by Heavy-Ion
1231 Elastic Recoil Detection and liquid scintillation counting. Nucl. Instr. Meth. B.
1232 doi:10.1016/j.nimb.2009.09.020.
1233 Kretzoi, M., Pécsi, M. 1982. Pliocene and Quaternary chronostratigraphy and continental
1234 surface development of the Pannonian Basin. In: Pécsi, M (ed.) Quaternary Studies in
1235 Hungary, INQUA, Hungarian Academy of Sciences, Geogr. Res. Inst., Budapest, 11-42.

Krolopp, E. 1995. Biostratigraphic division of Pleistocene formations in Hungary according to their mollusc fauna. In: Fűköh, L.; Krolopp, E.; Sümegi, P. 1995. Quaternary Malacostratigraphy in Hungary. Malacological Newsletter, Suppl. 1. Gyöngyös, pp. 17-78.

Lal, D. 1991. Cosmic ray labelling of erosion surfaces: in situ nuclide production rates and erosion rates. Earth and Planet. Sci. Lett. 104, 424-439.

Lian, O.B., Roberts, R.G., 2006. Dating the Quaternary: progress in luminescence dating of sediments. Quaternary Science Reviews 25, 2449–2468.

Lisiecki, L. E., and Raymo, M.E. 2005. A Pliocene-Pleistocene stack of 57 globally distributed benthic $\delta^{18}O$ records, Paleoceanography 20, PA1003, doi:10.1029/2004PA001071.

Lowick, S., Trauerstein, M., Preusser, F., 2012. Testing the application of post IR-IRSL dating to fine grain waterlain sediments. Quaternary Geochronology 8, 33-40.

Magyar, I., Lantos, M., Ujszászi, K., Kordos, L. 2007: Magnetostratigraphic, seismic and biostratigraphic correlations of the Upper Miocene sediments in the northwestern Pannonian Basin System. Geologica Carpathica 58, 277-290.

Magyar, I., Radivojević, D., Sztanó, O., Synak, R., Ujszászi, K., Pócsik, M. 2013. Progradation of the paleo-Danube shelf margin across the Pannonian Basin during the Late Miocene and Early Pliocene. Global and Planetary Change 103, 168-173.

Matsuoka, N. 2011. Climate and material controls on periglacial soil processes: Toward improving periglacial climate indicators. Quaternary Research 75, 356-365.

Matsushi, Y., Wakasa, S. Matsuzaki, H., Matsukura, Y. 2006. Long-term denudation rates of actively uplifting hillcrests in the Boso Peninsula, Japan, estimated from depth profiling of in situ-produced cosmogenic ^{10}Be and ^{26}Al. Geomorphology 82, 283–294, doi:10.1016/j.geomorph. 2006.05.009.

Merchel, S., Herpers, U., 1999. An Update on Radiochemical Separation Techniques for the Determination of Long-Lived Radionuclides via Accelerator Mass Spectrometry, Radiochimica Acta 84, 215-219.

Murray, A.S., Wintle, A.G. 2003. The single aliquot regenerative dose protocol: potential for improvements in reliability. Radiation Measurements 37, 377-381.

Murray, A.S., Schmidt, E.D., Stevens, T., Buylaert, J-P, Marković, S.B., Tsukamoto, S., Frechen, M. 2014. Dating Middle Pleistocene loess from Stari Slankamen (Vojvodina, Serbia) — Limitations imposed by the saturation behaviour of an elevated temperature IRSL signal. Catena 117, 34-42.

1269 Novothny, Á., Frechen, M., Horváth, E., Wacha, L., Rolf, C. 2011. Investigating the
1270 penultimate and last glacial cycles of the Süttö loess section (Hungary) using luminescence
1271 dating, high-resolution grain size, and magnetic susceptibility data. Quaternary International
1272 234, 75-85.
1273 Nitychoruk, J., Bińka, K., Ruppert, H., Schneider J., 2006. Holsteinian Interglacial=Marine
1274 Isotope Stage 11? Quaternary Science Reviews 21-22, 2678-2681.
1275 Pécsi, M. 1959. Formation and geomorphology of the Danube valley in Hungary (in
1276 Hungarian with German summary). Akadémiai Kiadó, Budapest, 346. p.
1277 Pécsi, M. 1961: Periglacial soil deformation features in Hungary (in Hungarian, with German
1278 summary) – Földrajzi Közlemények 9, (85), 1–24.
1279 Pécsi, M., 1997. Szerkezeti és váztalajképződés Magyarországon (in Hungarian with English
1280 summary). Magyar Tudományos Akadémia, Budapest, Hungary. 296 pp., English abstract:
1281 The effect of the Quaternary periglacial processes on the relief and structural soil formation.
1282 Penck, A., Brückner, E., 1909. Die Alpen im Eiszeitalter. Tauchnitz, Leipzig.
1283 Peters, G., van Balen, R. 2007. Pleistocene tectonics inferred from fluvial terraces of the
1284 northern Upper Rhine Graben, Germany. Tectonophysics 430. 41–65.
1285 Plug, L.J., Gosse, J.C., McIntosh, J.J., Bigley, R., 2007. Attenuation of cosmic ray flux in
1286 temperate forest. Journal of Geophysical Research 112. doi:10.1029/2006JF000668.
1287 Portenga, E.W., Bierman, P.R. 2011. Understanding Earth's eroding surface with ^{10}Be. GSA
1288 Today 21, 8, 4-9.
1289 Prescott, J.R., Hutton, J. T. 1994. Cosmic ray contribution to dose rates for luminescence and
1290 ESR dating: large depth and long-term time variations. Radiation Measurements 23, 497-
1291 500.
1292 Rees-Jones, J. 1995. Optical dating of young sediments using fine-grain quartz. Ancient TL
1293 13, 9-14 .
1294 Reimann, T., Thomsen, K.J., Jain, M., Murray, A.S., Frechen, M. 2012. Single-grain dating of
1295 young sediments using the pIRIR signal from feldspar. Quaternary Geochronology 11, 28-
1296 41.
1297 Rixhon, G., Braucher, R., Bourlès, D., Siame, L., Bovy, B., Demoulin, A. 2011. Quaternary
1298 river incision in NE Ardennes (Belgium)-Insights from ^{10}Be/^{26}Al dating of river terraces.
1299 Quaternary Geochronology 6. 273-284.
1300 Rixhon, G., Bourlès, D., Braucher, R., Siame, L., Cordy, J-M., Demoulin, A. 2014. ^{10}Be
1301 dating of the Main Terrace level in the Ambléve valley (Ardennes, Belgium): new age

1302 constraint on the archaeological and palaeontological filling of the Belle-Roche palaeokarst.
1303 Boreas 43, 2, 528-542.
1304 Rodés, Á., Pallàs, R., Braucher R., Moreno, X., Masana, E., Bourlés, D.L. 2011. Effect of
1305 density uncertainties in cosmogenic ^{10}Be depth-profiles: Dating a cemented Pleistocene
1306 alluvial fan (Carboneras Fault, SE Iberia). Quaternary Geochronology 6, 186-194.
1307 Rodnight, H, G A T Duller, A G Wintle, and S Tooth (2006), Assessing the reproducibility
1308 and accuracy of optical dating of fluvial deposits, Quat. Geochronol. 1, 109-120.
1309 Rónai, A. 1974. Size of Quaternary vertical movements in Hungary (in Hungarian). Acta
1310 Geologica Hungarica 18. 39-44.
1311 Ruszkiczay-Rüdiger, Zs., Fodor, L., Bada, G., Leél-Össy, Sz., Horváth, E., Dunai, T.J. 2005a.
1312 Quantification of Quaternary vertical movements in the central Pannonian Basin: A review
1313 of chronologic data along the Danube River, Hungary. Tectonophysics 410, 1-4, 157-172.
1314 Ruszkiczay-Rüdiger, Zs., Dunai, T.J., Bada, G., Fodor, L., Horváth, E. 2005b. Middle to late
1315 Pleistocene uplift rate of the Hungarian Mountain Range at the Danube Bend (Pannonian
1316 Basin) using in situ produced ^{3}He. Tectonophysics 410, 1-4, 173-187.
1317 Ruszkiczay-Rüdiger, Zs., Fodor, L., Horváth, E. 2007. Neotectonics and Quaternary
1318 landscape evolution of the Gödöllő Hills, Central Pannonian Basin, Hungary. Global and
1319 Planetary Change 58, 181-196.
1320 Ruszkiczay-Rüdiger, Zs., Braucher, R., Csillag, G., Fodor, L., Dunai, T.J., Bada, G., Bourlés,
1321 D., Müller, P. 2011. Dating pleistocene aeolian landforms in Hungary, Central Europe,
1322 using in situ produced cosmogenic ^{10}Be. Quaternary Geochronology 6, 515-529.
1323 Ruszkiczay-Rüdiger, Zs., Kern, Z. 2015. Permafrost or seasonal frost? - A review of
1324 paleoclimate proxies of the last glacial cycle in the East Central European lowlands.
1325 (accepted manuscript) Quaternary International.
1326 Schatz, A.K., Buylaert, J-P., Murray, A.S., Stevens, T., Scholten, T. 2012. Establishing a
1327 luminescence chronology for a palaeosol-loess profile at Tokaj (Hungary): A comparison of
1328 quartz OSL and polymineral IRSL signals. Quaternary Geochronology 10, 68-74.
1329 Schaller, M., von Blanckenburg, F., Hovius, N., Kubik, P., 2001. Large-scale erosion rates
1330 from in situ-produced cosmogenic nuclides in european river sediments. Earth and Planetary
1331 Science Letters 188, 441-458.
1332 Schaller, M., von Blanckenburg, F., Veldkamp, A., Tebbens, L.A., Hovius, N., Kubik, P.W.
1333 2002. A 30,000 yr record of erosion rates from cosmogenic ^{10}Be in Middle European river
1334 terraces, Earth Planet. Sci. Lett. 204. 307–320.

1335 Schmidt, S., Hetzel, R., Kuhlmann, J., Mingorance, F., Ramos, V.A., 2011. A note of caution
1336 on the use of boulders for exposure dating of depositional surfaces. Earth and Planetary
1337 Science Letters 302, 60–70.
1338 Schumm, S.A., Dumont, J.F., Holbrook, J.M. 2002. Active Tectonics and Alluvial Rivers.
1339 Cambridge University Press, 276 p.
1340 Sebe, K., Csillag, G., Ruszkiczay-Rüdiger, Zs., Fodor, L., Thamó-Bozsó, E., Müller, P.,
1341 Braucher, R. 2011. Wind erosion under cold climate: A fossil periglacial mega-yardang
1342 system in Central Europe (Western Pannonian Basin, Hungary). Geomorphology 134, 470-
1343 482.
1344 Siame, L., Bellier, O., Braucher, R., Se´ brier, M., Cushing, M., Bourle` s, D.L., Hamelin, B.,
1345 Baroux, E., de Voogd, B., Raisbeck, G., Yiou, F., 2004. Local erosion rates versus active
1346 tectonics: cosmic ray exposure modelling in Provence (South-East France). Earth and
1347 Planetary Science Letters 220 (3–4), 345–364.
1348 Sierralta, M., Kele, S., Melcher, F., Hambach, U., Reinders, J., van Geldern, R., Frechen, M.
1349 2009. Uranium-series dating of travertine from Süttő: Implications for reconstruction of
1350 environmental change in Hungary. Quaternary International 222, 1-2, 178-193.
1351 Stange, K.M., van Balen, R.T., Carcaillet, J., Vandenberghe, J., 2013. Terrace staircase
1352 development in the Southern Pyrenees Foreland: Inferences from ^{10}Be terrace exposure ages
1353 at the Segre River. Global and Planetary Change 101, 97–112.
1354 Stange, K.M., van Balen, R.T., Kasse, C., Vandenberghe, J., Carcaillet, J. 2014. Linking
1355 morphology across the glaciofluvial interface: A ^{10}Be supported chronology of glacier
1356 advances and terrace formation in the Garonne River, northern Pyrenees, France.
1357 Geomorphology 207, 71–95.
1358 Stevens, T., Marković, S.B., Zech, M., Hambach, U., Sümegi, P., 2011. Dust deposition and
1359 climate in the Carpathian Basin over an independently dated last glacial–interglacial cycle.
1360 Quaternary Science Reviews 30, 662–681.
1361 Stone, J.O., 2000. Air pressure and cosmogenic isotope production. Journal of Geophysical
1362 Research 105 (B10), 23753–23759.
1363 Szádeczky-Kardoss, E. 1938. Geologie der rumpfungarländischen kleinen Tiefebene. Sopron.
1364 444 p.
1365 Szádeczky-Kardoss, E. 1941. Ancient rivers in Transdanubia (in Hungarian). Földrajzi
1366 Értesítő 6/1, 119-134.

Szanyi, Gy., Surányi, G., Leél-Össy, Sz. 2012. Cave development and Quaternary uplift history in the Central Pannonian Basin derived from speleothem ages. Quaternary Geochronology 14, 18-25.

Szeberényi, J. 2014. Geomorphological horizons of the SE Börzsöny and Visegrád Gorge (in Hungarian). PhD Thesis, University of Pécs, 129. pp

Tari, G. 1994. Alpine tectonics of the Pannonian basin. PhS Thesis, Rice University, Texas USA, 501 p.,

Thamó-Bozsó, E., Csillag, G., Fodor, L.I., Müller, P.M., Nagy, A. 2010. OSL-dating the Quaternary landscape evolution in the Vértes Hills forelands (Hungary). Quaternary Geochronology 5. 120–124.

Thiel, C., Buylaert, J.-P., Murray, A., Terhorst, B., Hofer, I., Tsukamoto, S., Frechen, M. 2011. Luminescence dating of the Stratzing loess profile (Austria) - Testing the potential of an elevated temperature post-IR IRSL protocol. Quaternary International 234, 23-31.

Thiel, C., Horváth, E., Frechen, M. 2014. Revisiting the loess/palaeosol sequence in Paks, Hungary: A post-IR IRSL based chronology for the 'Younger Loess Series'. Quaternary International 319, 88-98.

Trauerstein, M., Lowick, S.E., Preusser, F., Schlunegger, F. 2014. Small aliquot and single grain IRSL and post-IR IRSL dating of fluvial and alluvial sediments from the Pativilca valley, Peru. Quaternary Geochronology 22, 163-174.

Uhrin, A., Sztanó, O., Csillag, G., Hámori, Z. 2011. Pliocene rivers in the south-eastern foreland of the Vértes Hills (in Hungarian with English summary). Földtani Közlöny 141/4, 363-382

Van Vliet-Lanoë, B., Magyari, Á. & Meilliez, F. 2004. Distinguishing between tectonic and periglacial deformations of Quaternary continental deposits in Europe. Global and Planetary Change 43, 103–127.

Vermeesch, P., 2007. CosmoCalc: an Excel add-in for cosmogenic nuclide calculations. Geochemistry, Geophysics, and Geosystems 8. doi:10.1029/ 2006GC001530 Q08003

Viveen, W. Braucher, R., Bourlès, D., Schoorl, J.M., Veldkamp, A., van Balen, R.T., Wallinga,. Fernandez-Mosquera, D., Vidal-Romani, J.R., Sanjurjo-Sanchez, J. 2012. A 0.65 Ma chronology and incision rate assessment of the NW Iberian Miño River terraces based on ^{10}Be and luminescence dating. Global and Planetary Change 94-95, 82–100.

Ward, D.J., Spotila, J.A., Hancock, G.S., Galbraith, J.M. 2005. New constraints on the late Cenozoic incision history of the New River, Virginia. Geomorphology 72, 54– 72.

1400 Warner, R.F. 2012. A Morphological Study of Durance River Terraces from Tallard to
1401 Avignon, South-East France. Central European Journal of Geosciences 4(3), 357-375.
1402 Wintle, A.G. 1973. Anomalous fading of thermoluminescence in mineral samples, Nature
1403 245, 143–144.
1404 Wintle, A. G. 2008. Luminescence dating: where it has been and where it is going. Boreas 37,
1405 471–482.
1406 Wintle, A.G., Murray, A.S. 2006. A review of quartz optically stimulated luminescence
1407 characteristics and their relevance in single-aliquot regeneration dating protocols. Radiation
1408 Measurements 41, 369-391.
1409 Wolkowinsky, A.J., Granger, D.E. 2004 Early Pleistocene incision of the San Juan River,
1410 Utah, dated with ^{26}Al and ^{10}Be. Geology 32/9, 749-752.
1411 Ziegler, P.A., Dézes, P. 2007. Cenozoic uplift of Variscan Massifs in the Alpine foreland:
1412 Timing and controlling mechanisms. Global and Planetary Change 58, 237–269.
1413
1414
1415 **Figure captions**
1416
1417 **Fig. 1.** SRTM-based digital elevation model of the Western Pannonian Basin and schematic
1418 pattern of neotectonic deformation structures (after Fodor et al, 2005; Bada et al, 2007;
1419 Dombrádi et al, 2010; Ruszkiczay-Rüdiger et al., 2007). DB: Danube Bend; GTT: Győr-
1420 Tata terrace region, W: location of ^{10}Be exposure age dated, 1.56±0.09 Ma old wind
1421 polished landforms (Ruszkiczay-Rüdiger et al, 2011).
1422
1423 **Fig. 2A.** Terraces at the marginal zones of the Danube Basin. Terraces in the western side of
1424 the DB were tentatively mapped using the Surface geological map of the DANREG
1425 project (Császár et al., 2000). Rectangles show the locations of the multielectrode
1426 resistivity (MUEL) profiles of Fig. 10. Sample locations: Gy: Győr; B: Bana; Á: Ács; M:
1427 Mocsa; Gr: Grébics. VB: Vienna Basin, EA: Eastern Alps, TR: Transdanubian Range, G.
1428 Gerecse Hills.
1429 **Fig. 2B.** Simplified geological cross section of the central part of the Győr-Tata terraces
1430 (modified after Pécsi, 1959). Location appears on Fig. 2A. Black dots indicate sample sites
1431 (depth profiles at Ács and Bana).
1432

Fig. 3. Longitudinal sketch of the terrace levels along the Danube from the Danube Basin to the Great Hungarian Plain (modified after Pécsi, 1959). Variations of the elevation of the horizons indicate Quaternary vertical deformation (orange arrow: uplift, yellow arrow: subsidence). The study area, the Győr-Tata terraces (GTT, light red shadow) is in the marginal zone of the uplifting Transdanubian Range. The Danube Bend (DB) is at the axial zone of the uplifting area characterised by most intensive uplift. Dotted lines indicate subsurface horizons. Levels below tIIb do not appear in the figure. For location see Fig.1. Sample sites appear with capital letters as in Fig.2A.

Fig.4. Periods of terrace formation in the Hungarian Danube valley according to previous studies and results of this study plotted above the benthic $\delta^{18}O$ record and MIS stages (Lisiecki and Raymo, 2005).

Fig. 5. Field images of the sample sites. A: Győr; B: Bana, C: Grébics, D/1: Mocsa gravel pit (TCN samples), D/2 Mocsa, sand pit (postIR-IRSL samples) E: Ács. For sample codes refer to Table 2 and Fig. 6. The TCN samples of the Mocsa profile (D/1) were taken in a gravel pit 1 km away from the postIR-IRSL location in a sand pit of the same terrace horizon (D/2). BanaB3 and Ács B3 postIR-IRSL samples were collected from the fine sand underlying the terrace material ~20 meters away from the depth profiles. Hence these samples do not appear on the photos. Zero point of the scale-bar indicates the original surface.

Fig. 6. The sampled terrace profiles with TCN and post-IR IRSL sample locations. Post-IR IRSL samples of the Mocsa profile were taken in a sand quarry of the same terrace horizon 1 km away from the TCN location (Mocsa1 and -2 profiles). BanaB3 and Ács B3 IRSL samples were collected from the underlying late Miocene fine sand ~20 meters away from the depth profiles from the underlying fine sand. These samples were not considered for the age determination of the terraces.

Fig. 7. Measured ^{10}Be concentrations plotted against sample depth. Black square of the subset C (Grébics) shows the average ^{10}Be concentration of the mixed upper horizon. Pebbles means amalgamated pebble sample. Error bars of 1σ analytical uncertainty remain invisible where they are within the size of the symbols.

Fig. 8. Representative examples for not saturated dose-response curves: samples Ács-A1 (A) and Mocsa-1 (B). Sample Bana-B3 (C) has reached saturation level.

Fig.9. Small aliquot De distributions determined with the pIRIR-290 protocol for sub-samples of Mocsa-1, Mocsa-2, Ács-A2 and Ács-4.

Fig. 10. MUEL profiles on terrace tIV-VI horizon. For locations refer to Fig. 2A. Coarse grained sediments, gravel and sandy gravel layers appear with high resistivity values (>100 Ωm). Small resistivity values are indicative of fine sediments like fine sand and silt (<40 Ωm). MUEL measurements were calibrated by shallow boreholes and outcrop evidences. MUEL survey was done by the Geomega Ltd. in 2004.

Fig. 11. Uplift rates along the Danube using different proxies.

[1] this study; [2] Pécsi (1959), Ruszkiczay-Rüdiger et al. (2005a) and this study, for terraces up to tIV (420 ka), and the subsidence rate in the Danube Basin was calculated using 400 m thickness of Quaternary strata (Rónai, 1974); [3] Kele, 2009, Sierralta et al (2009); [4] Szanyi et al. (2012); [5] Ruszkiczay-Rüdiger et al. (2005b); [6] Grenerczy et al. (2005). Note the break in the vertical axis above 0.6 mm/a.

The ^{10}Be dating-based trend of incision rates was based on the >700 ka age of the onset of valley incision suggested by the ^{10}Be exposure age of the highest terrace level (tIV-VI) of the study area (yellow shading), which was tentatively extrapolated to the entire TR section of the Danube valley (dotted line). See details in the text. Uplift rate data are presented in Table S7.

Table captions appear in a separate file together with the tables

Table

	incision/uplift rate (mm/a)	dated landform	method	location	timespan (ka)
Antón et al. (2012)	2.0-3.0	strath terraces	cosmogenic ^{10}Be, ^{21}Ne	Duero Basin	100-0
Brocard et al. (2003)	0.8	alluvial terraces	cosmogenic ^{10}Be	French Western Alps	190-0
Giachetta et al. (2015)	0.25-0.55	-	numerical modeling	Iberian Chain	3000-0
Häuselmann et al. (2007a)	~0.12 ~1.2	cave sediments	cosmogenic ^{10}Be, ^{26}Al	Switzerland	>800 800-0
Necea et al. (2013)	0.1-2.2	alluvial terraces	IRSL	SE Carpathians	780-0
Peters and van Balen (2007)	0.01-0.16	alluvial terraces	correlation, relative chronology	Upper Rhine Graben	800-0
Rixhon et al. (2011, 2014)	0.08-0.14*	alluvial terraces	cosmogenic ^{10}Be	NE Ardennes	725-0
Viveen et al. (2012)	0.07-0.08	alluvial terraces	cosmogenic ^{10}Be, OSL, IRSL	Miño River, Iberia	650-0
Wagner et al. (2010)	0.1	cave sediments	cosmogenic ^{10}Be, ^{26}Al	Eastern Alps	4000-0
Ziegler-Dézes (2007)	1.75	-	geodetic data	Variscan Massifs in the Alpine foreland	2600-0
this study**	<0.06-0.13 (up to 0.33***)	alluvial terraces	cosmogenic ^{10}Be	Danube River	>700-0
this study	0.13-0.15	alluvial terraces	post-IR IRSL	Danube River	140-0

Table 1. Some incision/uplift rates derived from terrace studies and geodetic data in Europe.
* The incision/uplift rate was calculated by this study based on the data published by Rixhon et al. (2011, 2014).
** The exposure ages are minimum ages therefore the incision/uplift rates are maximum rates.
*** Incision/uplift rate inferred by data extrapolation along the valley.

Sample	Location	Latitude (DD)	Longitude (DD)	Alt. asl. /amrl (m)	Thick-ness (cm)	Depth (cm)*	Mass od quartz dissolved (g)	[^{10}Be] concentration (atoms/g)		max. denudation rate (m/Ma)	
Dan08-02s	Győr	47.6582	17.7251	147	7	49	34.5131	369 537	±11 710	5.8	±0.2
Dan08-03s	Győr			/38	7	79	35.4654	292 737	±7 891	5.3	±0.1
Dan08-04s	Győr				7	109	33.0804	230 199	±10 362	4.9	±0.2
Dan08-04p	Győr				7	109	39.0470	199 552	±5 246	5.9	±0.2
Dan08-05s	Győr				7	139	37.5003	200 303	±5 130	4.1	±0.1
Dan08-05p	Győr				7	139	42.0290	158 609	±5 429	5.7	±0.2
Dan08-06s	Győr				7	184	36.4694	118 567	±5 284	5.3	±0.2
Dan08-06p	Győr				7	184	41.5389	110 608	±6 288	5.9	±0.3
Dan08-07s	Győr				7	234	40.0643	133 263	±3 412	2.5	±0.1
Dan08-08s	Győr				7	284	40.2015	88 745	±4 943	3.3	±0.2
Dan08-09s	Győr				7	334	41.1239	87 704	±2 241	2.1	±0.1
Dan08-09p	Győr				7	334	42.3270	73 809	±2 764	3.4	±0.1
Dan08-10p	Győr				7	394	44.5935	71 048	±1 783	2.4	±0.1
Dan08-11s	Győr				7	484	39.9080	36 908	±1 489	10.0	±0.4
Dan08-12s	Győr				7	750	40.7842	16 058	±554	30.7	±1.1
Dan08-20p	Bana	47.6749	17.88614	153	8	0	39.4791	430 686	±14 233	8.9	±0.3
Dan08-21p	Bana			/45	8	22.5	40.5013	339 089	±9 589	8.8	±0.3
Dan08-22p	Bana				8	67.5	43.9504	329 116	±9 450	5.3	±0.2
Dan08-23p	Bana				8	142.5	46.0544	136 767	±4 210	6.7	±0.2
Dan08-24p	Bana				8	255	44.0128	99 823	±4 752	3.4	±0.2
Dan08-25p	Bana				8	375	44.6229	102 889	±2 986	0.7	±0.0
Dan08-26s	Bana				8	425	40.8223	77 599	±6 185	1.3	±0.1
Dan08-27p	Ács (actual)	47.7447	18.00424	108 /0	3	0	39.9286	81 254	±2 335	52.7	±1.5
Dan08-31p	Mocsa	47.6792	18.2133	127	6	135	41.0265	197 414	±6 086	5.3	±0.2
Dan08-32p	Mocsa			/20	6	185	44.1590	113 208	±3 299	6.6	±0.2
Dan08-33p	Mocsa				6	245	41.3162	100 597	±3 196	4.4	±0.1
Dan08-34p	Mocsa				6	305	46.2831	106 516	±3 276	2.1	±0.1
Dan08-35p	Mocsa				6	405	41.9937	98 208	±3 928	0.7	±0.0
Dan08-40p	Grébics	47.6588	18.2580	194	8	5	41.9371	340 904	±12 575	11.7	±0.4
Dan08-41p	Grébics			/87	8	40	41.4907	472 052	±16 606	5.1	±0.2
*Dan08-40-41 avg***	*Grébics*				*8*	*22*	-	*406 478*	*±16 606*	*7.5*	*±0.3*
Dan08-42p	Grébics				8	80	40.5622	223 208	±8 519	7.5	±0.3
Dan08-43p	Grébics				8	115	40.8454	176 707	±6 216	6.7	±0.2
Dan08-44p	Grébics				8	155	41.4021	157 497	±6 442	5.0	±0.2
Dan08-45p	Grébics				8	195	40.5254	107 100	±3 793	5.7	±0.2
Dan08-46p	Grébics				8	225	40.4120	103 398	±5 173	4.5	±0.2
Dan13-07fs	Ács	47.7425	18.0064	121	6	10	24.6485	77 385	±6 704	55.9	±4.8
Dan13-08fs	Ács			/12	6	33	22.4840	83 135	±10 860	41.8	±5.5
Dan13-09fs	Ács				6	63	23.9188	93 930	±7 401	27.8	±2.2
Dan13-10fs	Ács				6	113	21.9429	83 537	±6 148	20.5	±1.5
Dan13-11s	Ács				8	135	15.3875	142 269	±8 877	8.8	±0.6
Dan13-12s	Ács				8	165	15.7705	137 354	±4 827	6.7	±0.2
Dan13-13ps	Ács				8	195	16.2782	132 721	±5 654	5.1	±0.2
Dan13-14s	Ács				8	235	15.7782	132 957	±4 804	3.2	±0.1
Dan13-15ps	Ács				8	275	14.8034	137 143	±5 768	1.9	±0.1
Dan13-16ps	Ács				8	325	16.0647	127 170	±7 210	1.1	±0.1
Dan13-17ps	Ács				8	360	15.2088	119 417	±5 157	0.8	±0.0
Dan13-18ps	Ács				8	400	15.6942	139 288	±6 217	0.1	±0.0

Table 2. Samples sites and cosmogenic ^{10}Be data. Samples were corrected for self-shielding. Topographic shielding factor is 1 for all sites. ^{10}Be/^{9}Be ratios of process blanks were (3.07 ± 0.7) × 10^{-15} (for samples Dan08-02 to-12); (1.23±0.4) × 10^{-15} (samples Dan08-20 to -46), and (2.37±0.7) × 10^{-15} (samples Dan13-07 to -18). Ages and denudation rates were not corrected for geomagnetic variations. Alt. asl/amrl: Altitude above sea level/above mean river level; s: sand sample, p: amalgamated pebbles; fs: fine-sand, ps: mixed sand and amalgamated pebbles.

* mean depth of the sample;
**Sample depth and ^{10}Be concentration calculated as the arithmetic mean of the depths and ^{10}Be concentrations of samples Dan08-40 and -41.

Threshods	Győr (p)	Győr (s)	Bana	Grébics	Mocsa	Ács*
χ^2 cutoff	2	15	6.5	5	31	<2.5**
min erosion rate (cm/ka)	0.2	0.2	0.5	0.2	0.1	0.0
max erosion rate (cm/ka)	1.2	1.0	1.5	1.4	1.2	1.0
total erosion min. (cm)	500	500	500	600	1	0
total erosion max. (cm)	1500		1500	1600	500	500
min. age (ka)	150		150	150	14	0
max. age (ka)	2600		2600	2600	360	100
site specific spallogenic production rate (at/g/a)	4.6185		4.6415	4.8394	4.5398	4.5124

Table 3. Monte Carlo simulation parameters used for the depth profile simulator of Hidy et al (2010). 100 000 solutions were obtained for each simulation. Győr (p): amalgamated pebble samples; Győr (s): sand samples.
*Only the buried exposure time of the alluvial sediments could be simulated. See details in text.
** 2σ confidence level.

	age (ka)	*inheritance (10^3 at/ g)*	*denudation rate (m/Ma)*
Győr - pebble			
Bayesian most probable	1 561	70	6.5
Bayesian 2σ upper	2 450	97	9.3
Bayesian 2σ lower	693	59	5.1
Bayesian 1σ upper	2 064	84	8.0
Bayesian 1σ lower	993	65	5.8
Győr - sand			
Bayesian most probable	1 783	95	7.0
Bayesian 2σ upper	2 448	149	8.3
Bayesian 2σ lower	708	72	5.2
Bayesian 1σ upper	2 098	122	7.5
Bayesian 1σ lower	1 024	83	5.8
Bana			
Bayesian most probable	1242	106	10.0
Bayesian 2σ upper	1541	140	12.2
Bayesian 2σ lower	477	92	8.7
Bayesian 1σ upper	1332	127	11.1
Bayesian 1σ lower	640	100	9.4
Grébics			
Bayesian most probable	1482	85	8.7
Bayesian 2σ upper	2003	133	11.0
Bayesian 2σ lower	659	53	7.1
Bayesian 1σ upper	1696	109	9.8
Bayesian 1σ lower	883	70	7.8
Mocsa			
Bayesian most probable	149	91	5.8
Bayesian 2σ upper	352	99	10.4
Bayesian 2σ lower	99	83	1.3
Bayesian 1σ upper	309	95	7.9
Bayesian 1σ lower	136	87	3.1
Ács (buried exposure)			
Bayesian most probable	12	127	9.9
Bayesian 2σ upper	65	138	9.8
Bayesian 2σ lower	0	114	0.2
Bayesian 1σ upper	38	132	8.6
Bayesian 1σ lower	6	120	1.7

Table 4. Best constrained model solutions of the ^{10}Be depth profile simulator (Hidy et al., 2010). For simulation settings refer to Table 3. Complete data tables appear in Table S1). Bayesian 1σ and 2σ upper and lower values represent the 68 and 95 % uncertainties of the Bayesian most probable values.

Sample name	Depth [m]	Grain size [μm]	Dose rate [Gy/ka]	Equivalent dose [Gy] pIRIR- 290	Age [ka] pIRIR- 290	Saturation*
Bana-A1	4.1	150-250	2.26 ± 0.21	> 924.6	**> 410**	0.87
Bana-A2	4.6	200-250	2.56 ± 0.15	> 988.8	**> 386**	0.88
Bana-B3	10.4	150-200	3.40 ± 0.19	> 1119.1	**> 320**	0.95 ± 0.01
Mocsa-1	1.0	100-150	2.72 ± 0.17	380.0 ± 10.0	**139 ± 9**	
Mocsa-2	1.6	250-300	2.65 ± 0.17	386.8 ± 9.5	**146 ± 10**	
Ács-A1	1.0	150-200	3.03 ± 0.16	46.2 ± 3.2	**15.2 ± 1.3**	
Ács-A2	1.7	200-250	2.68 ± 0.15	253.1 ± 4.7	**95 ± 6**	
Ács-B3	8.4	150-200	3.51 ± 0.17	> 903.6	**> 258**	0.93 ± 0.02
Ács-A4	3.9	150-200	2.78 ± 0.15	238.0 ± 12.1	**86 ± 6**	

Table 5. Sample characteristics for coarse-grained K-feldspar post-IR IRSL-290 dating. Sample depth, grain size, dose rate, equivalent dose and corresponding age. *Saturation levels were measured on one aliquot/sample for Bana-A1 and A2, and on 3 aliquots/sample for Bana-B3 and Ács-B3. The data table for the pIRIR-225 protocol is Table S6.

	Győr-pebble	***Győr-sand***	***Bana***	***Grébics***	***Mocsa***	***Ács***
Exposure age (ka)	>693	>708	>477	>659<	149^{+160}_{-13}	–
Denudation rate (m/Ma)	$6.5^{+1.6}_{-0.7}$	$7.0^{+0.5}_{-1.2}$	$10.0^{+1.1}_{-0.6}$	$8.7^{+1.2}_{-0.8}$	$5.8^{-2.1}_{+2.6}$	–
Inheritance (10^3 at/g)	70^{+14}_{-5}	95^{+27}_{-12}	106^{+21}_{-6}	85^{+24}_{-15}	91^{+4}_{-4}	–
Post-IR IRSL age	–	–	>410	–	143±10*	91±6*
Terrace level (traditional **- this study)**	tIV - **tVI**	tIV - **tVI**	tIV - **tVI**	tIV - **tVI**	tIIb - **tIIIa**	**tIIb**
height above the Danube (m)	38	38	45	87	20	12

Table 6. Exposure time, denudation rate, inheritance and post IR IRSL age of the studied terraces. Bayesian most probable values, with a 1σ confidence window are presented. Minimum exposure ages are Bayesian 2σ lower ages. Height above Danube refer to the present elevation of the surface of the alluvial material.

* arithmetic mean of the measured ages in Table 5.

Figure1

Click here to download high resolution image

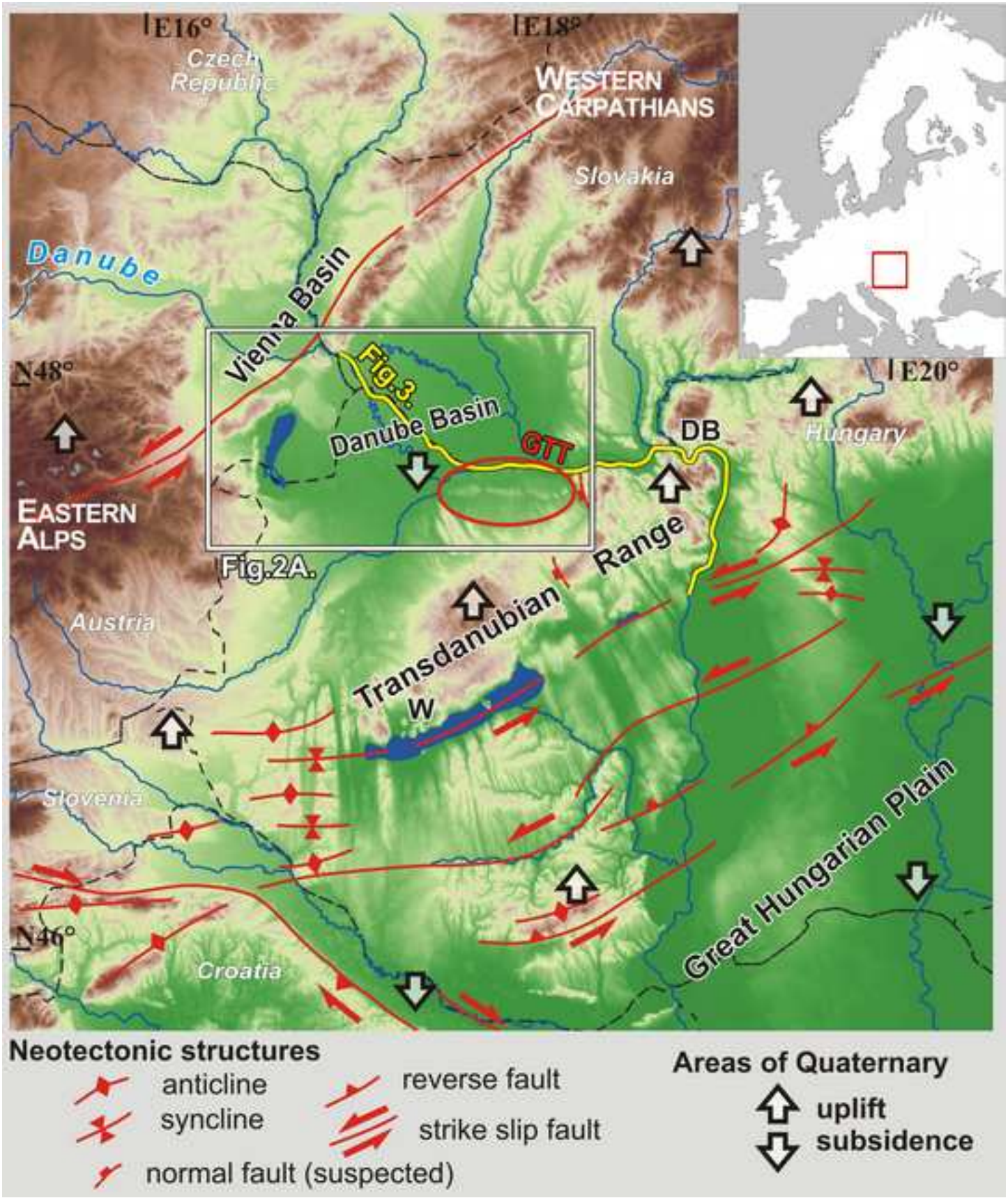

Figure2

Click here to download high resolution image

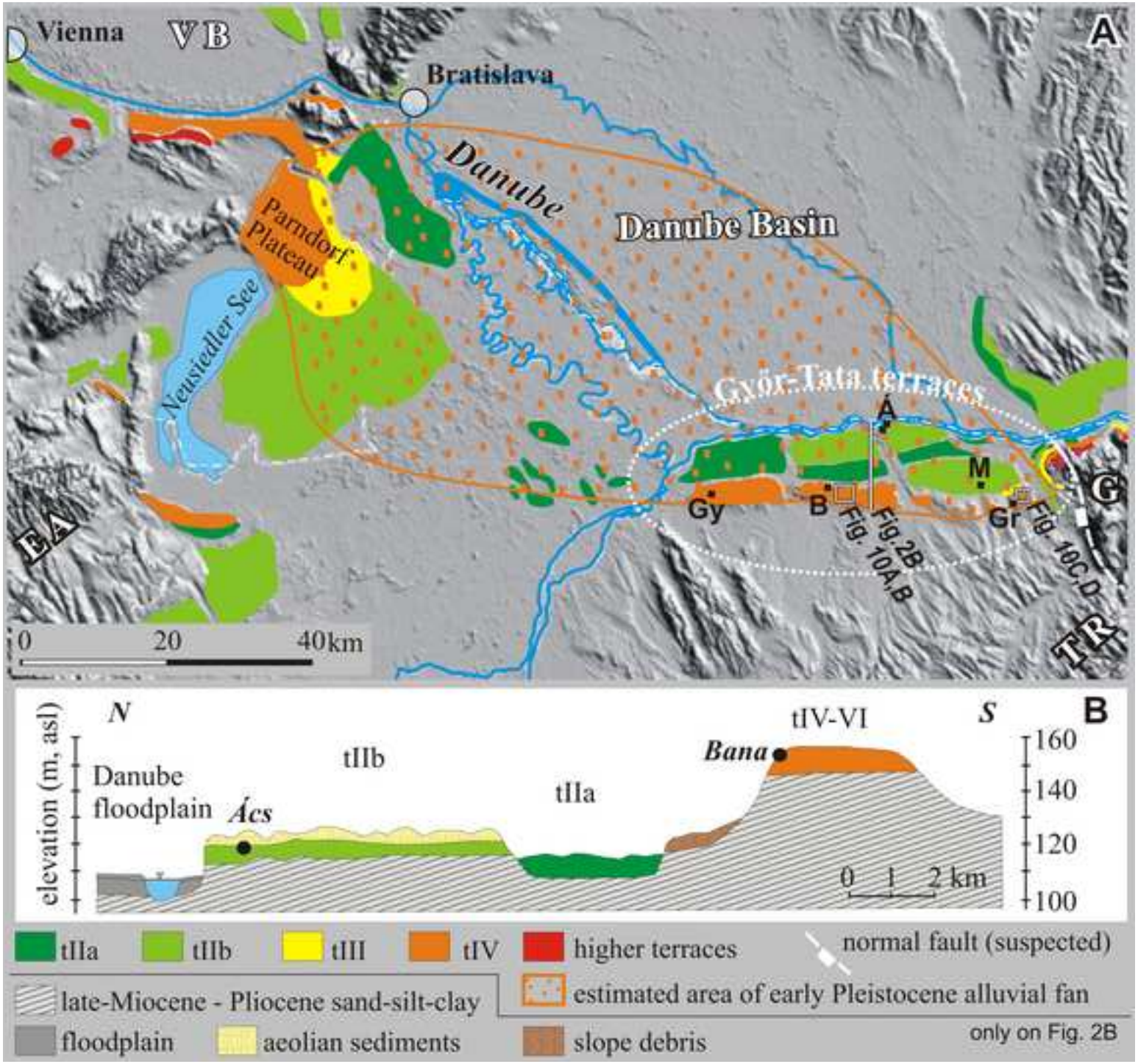

Figure3

Click here to download high resolution image

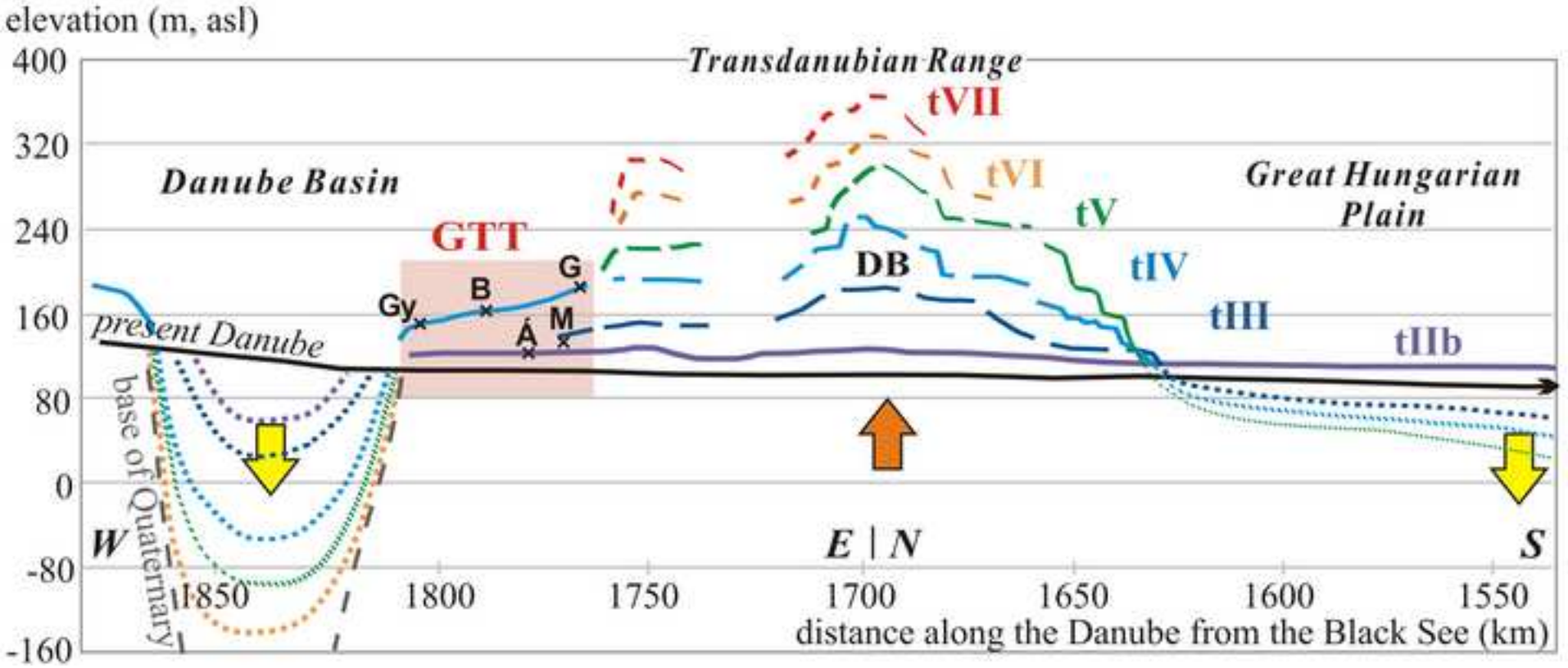

Figure4

Click here to download high resolution image

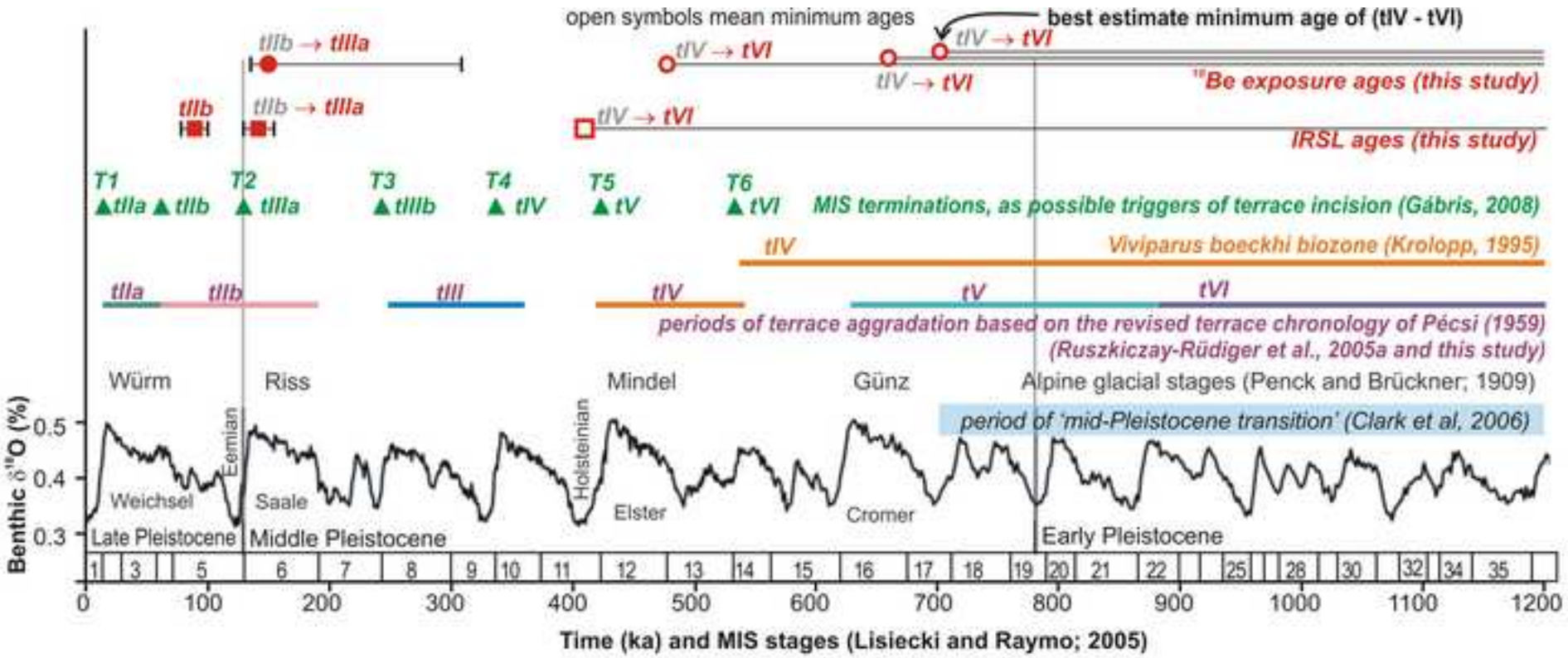

Figure5

Click here to download high resolution image

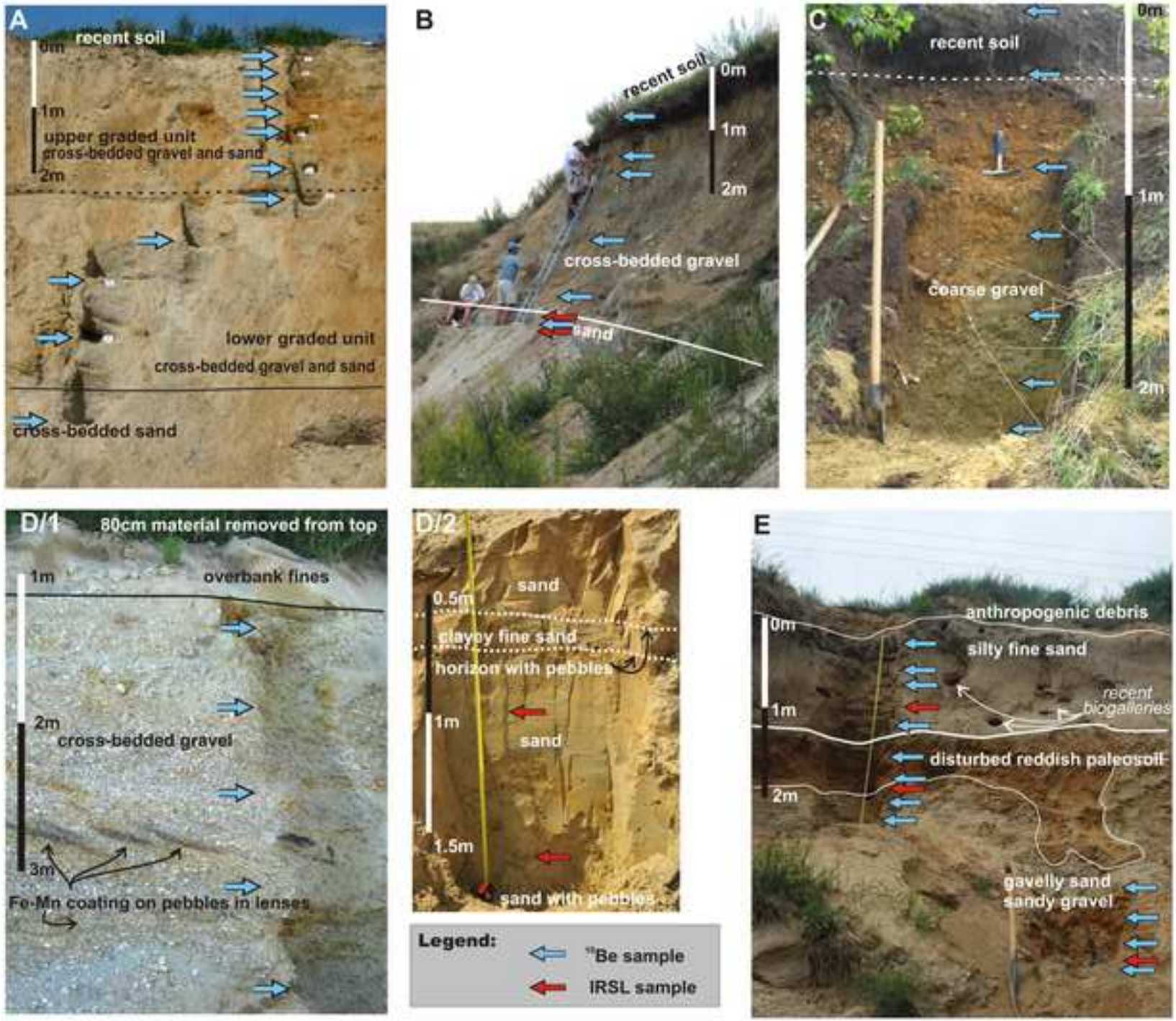

Figure6

Click here to download high resolution image

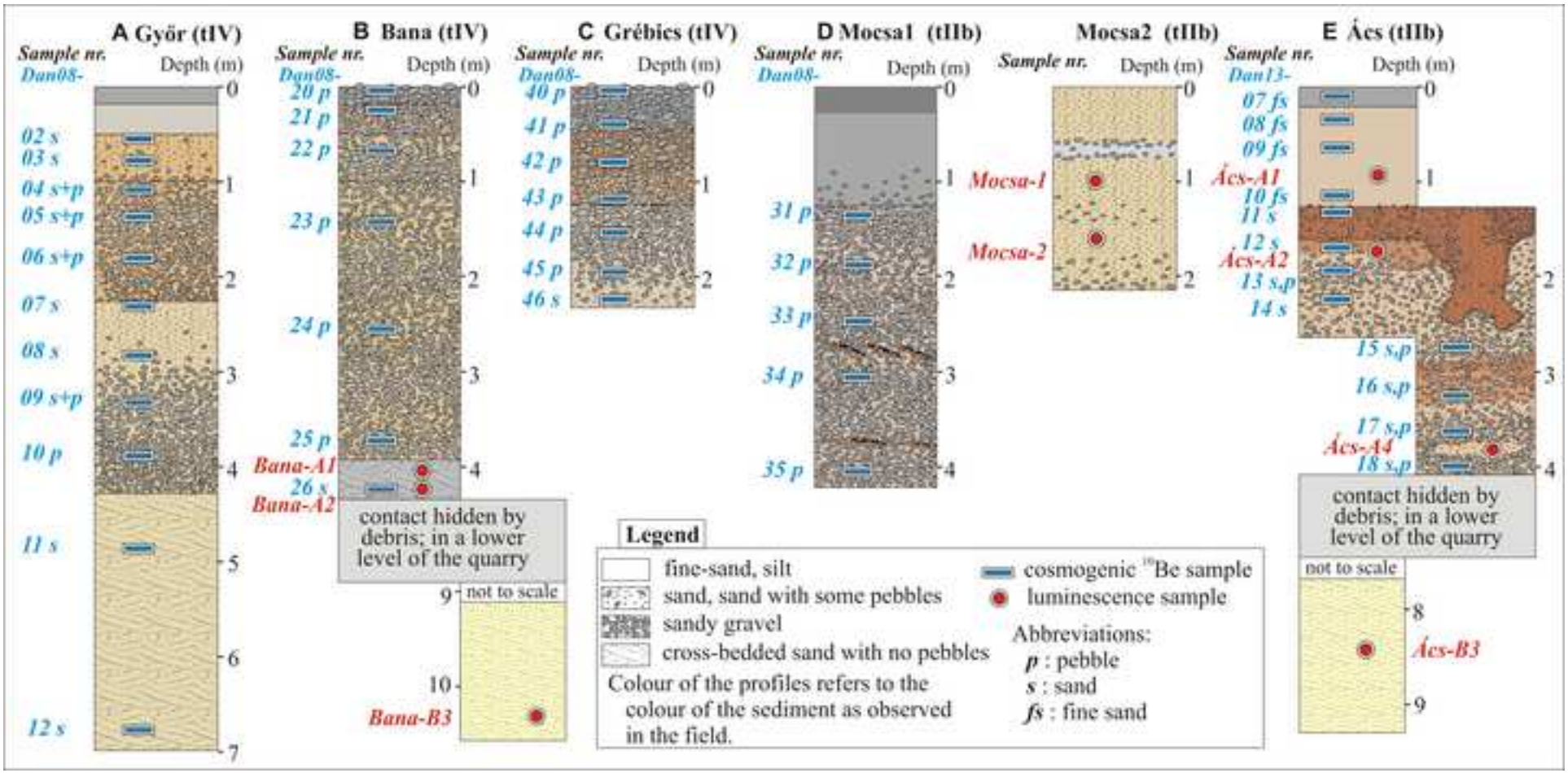

Figure7

Click here to download high resolution image

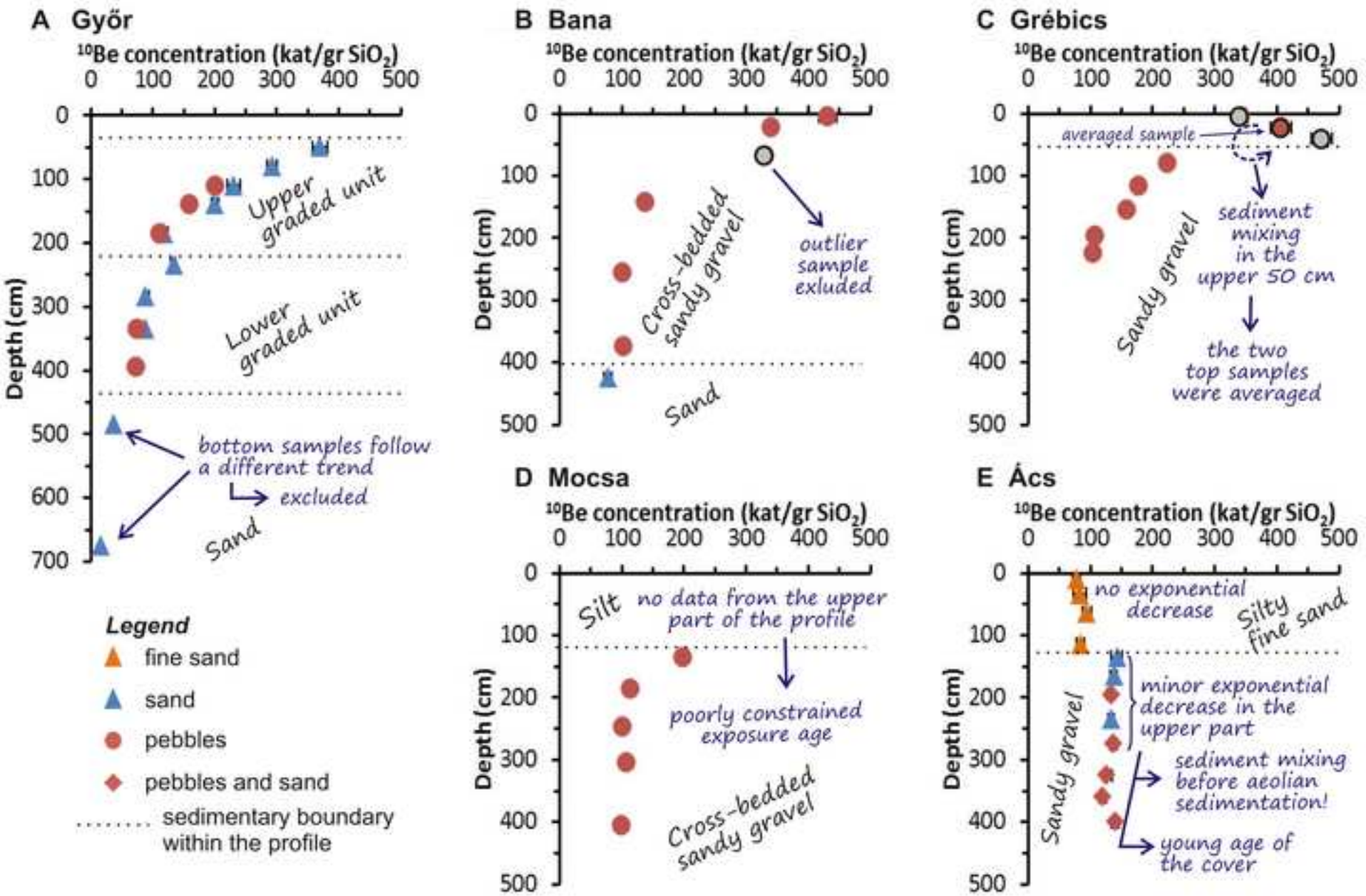

Figure8

Click here to download high resolution image

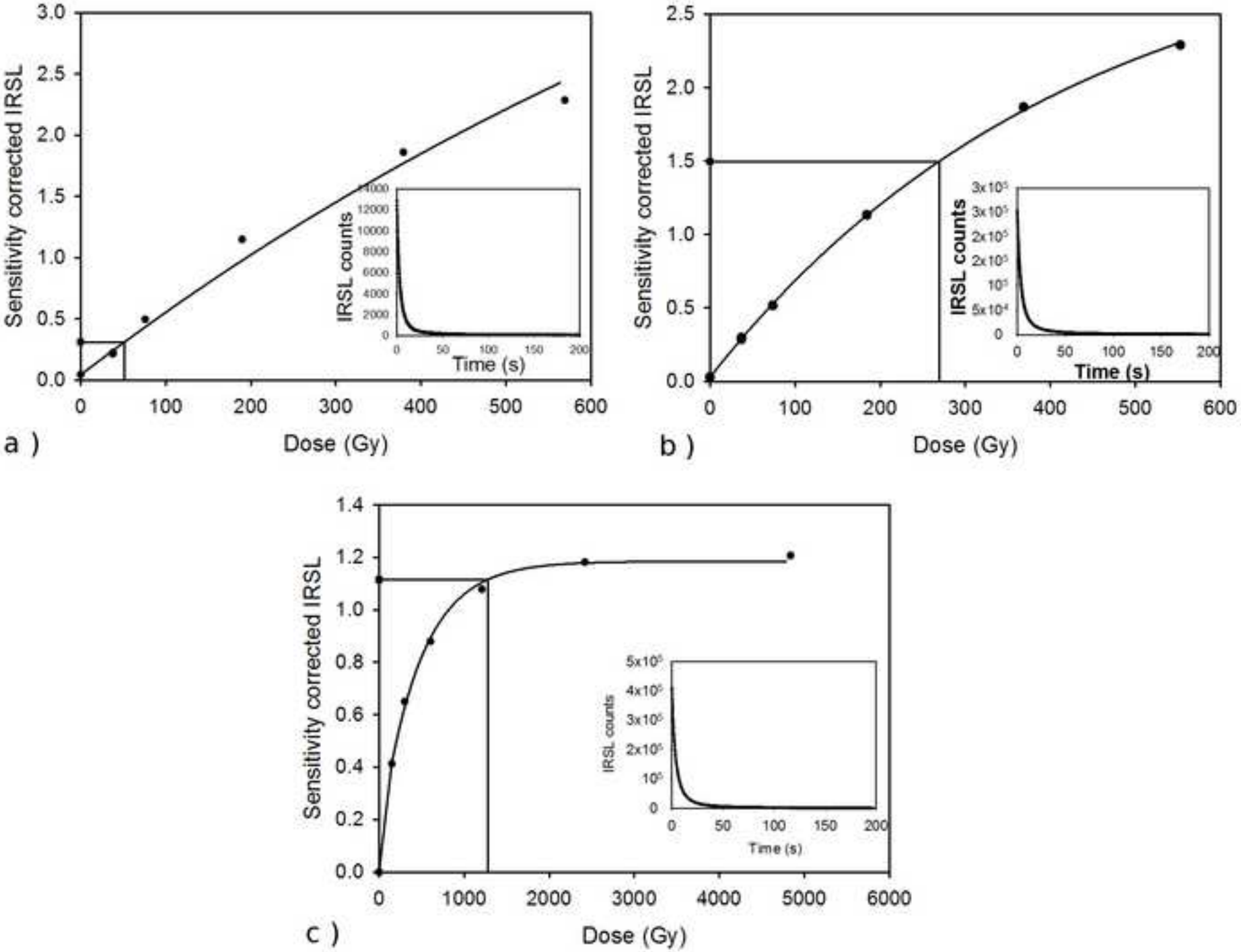

Figure9

Click here to download high resolution image

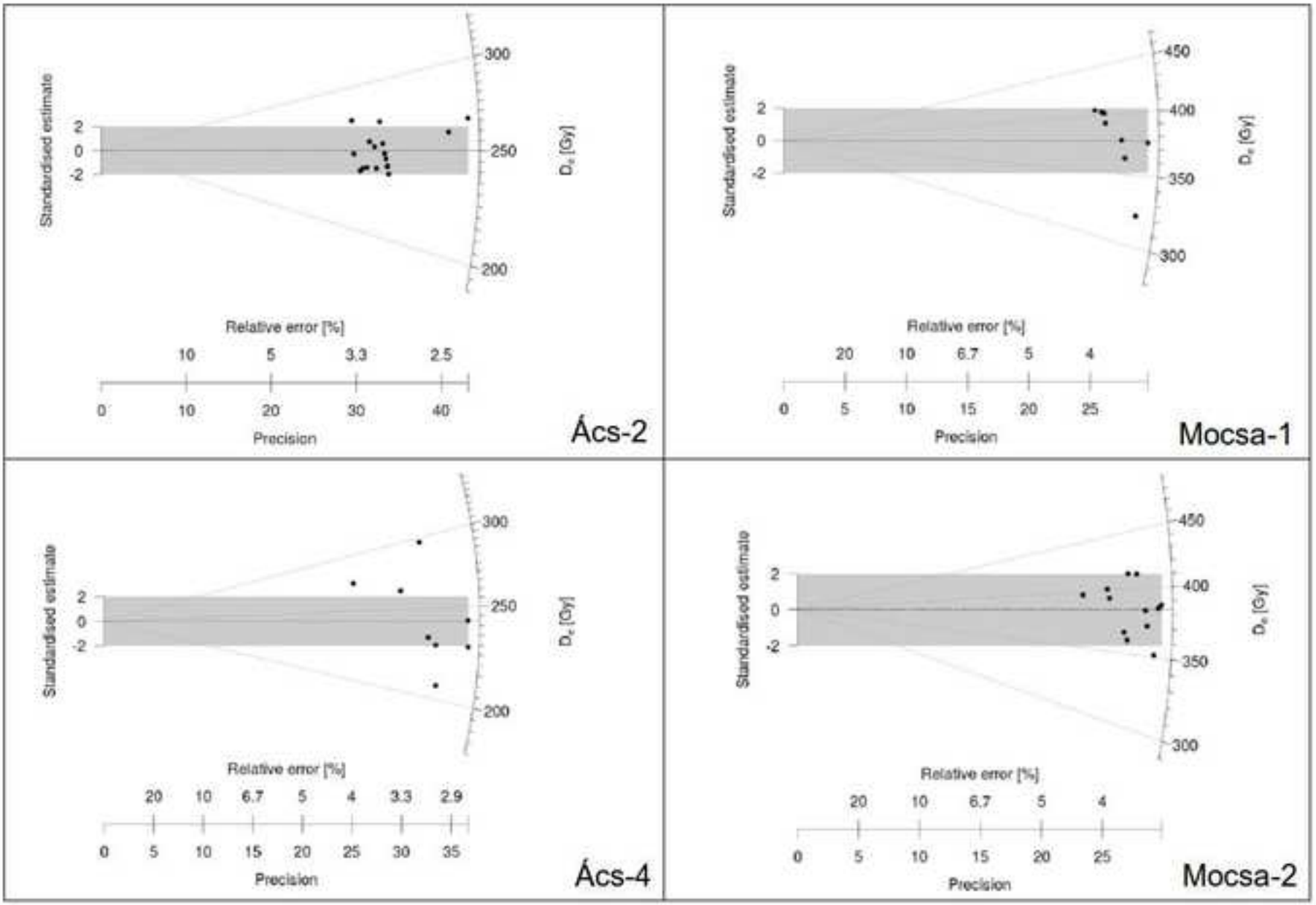

Figure10

Click here to download high resolution image

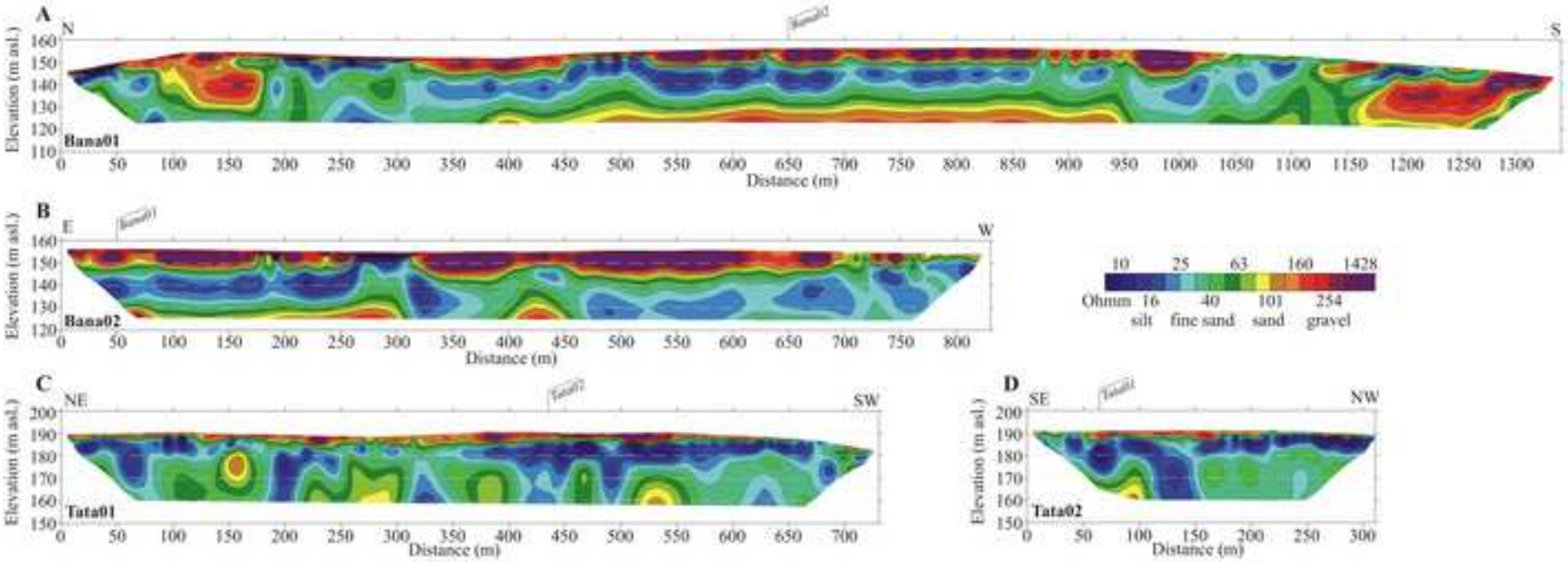

Figure11

Click here to download high resolution image

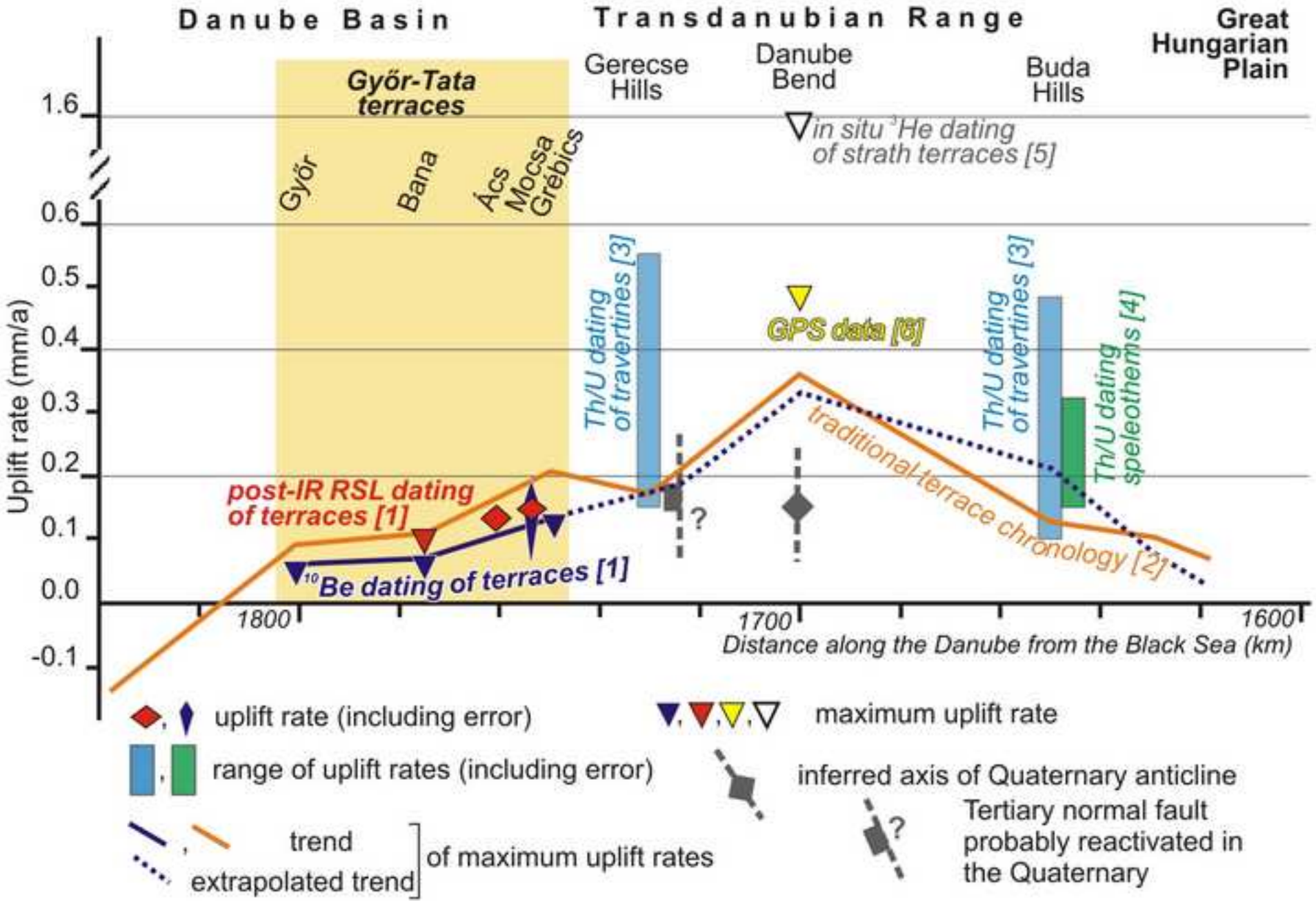

Supplementary information

Click here to download Supplementary Data: Ruszkiczay_etal_2015_QSR_Suppl_material.pdf

mathlab code1

Click here to download Supplementary Data: be_calcmuonproduction.m

mathlab code 2

Click here to download Supplementary Data: be_main.m

mathlab code 3

Click here to download Supplementary Data: be_muonproduction.m

mathlab code 4

Click here to download Supplementary Data: be_probfix3.m